Experimental Eye Research 116 (2013) 109–128

Contents lists available at ScienceDirect

Experimental Eye Research

journal homepage: www.elsevier.com/locate/yexer

The structure and development of *Xenopus laevis* cornea☆

Wanzhou Hu [a,1], Nasrin Haamedi [a,1], Jaehoon Lee [b], Tsutomu Kinoshita [b], Shin-ichi Ohnuma [a,*]

[a] UCL Institute of Ophthalmology, UCL, 11-43 Bath Street, London EC1V 9EL, UK
[b] Department of Life Science, Faculty of Science, Rikkyo University, 3-34-1 Nishi-Ikebukuro, Toshima-ku, Tokyo 171-8501, Japan

ARTICLE INFO

Article history:
Received 18 March 2013
Accepted in revised form 17 July 2013
Available online 27 July 2013

Keywords:
Xenopus
cornea
eye
embryo
development
amphibian
neural crest
metamorphosis
cell death

ABSTRACT

The African clawed frog, *Xenopus laevis*, is a widely used model organism for tissue development. We have followed the process of corneal development closely in *Xenopus* and examined the corneal ultrastructure at each stage during its formation. *Xenopus* cornea development starts at stage 25 from a simple embryonic epidermis overlying the developing optic vesicle. After detachment of the lens placode which takes place around stage 30, cranial neural crest cells start to invade the space between the lens and the embryonic epidermis to construct the corneal endothelium. At stage 41, a second wave of migratory cells containing presumptive keratocytes invades the matrix leading to the formation of inner cornea and outer cornea. Three-dimensional electron microscopic examination shows that a unique cell mass, the stroma attracting center, connects the two layers like the center pole of a tent. After stage 48, many secondary stromal keratocytes individually migrate to the center and form the stroma layer. At stage 60, the stroma space is largely filled by collagen lamellae and keratocytes, and the stroma attracting center disappears. At early metamorphosis, the embryonic epithelium gradually changes to the adult corneal epithelium, which is covered by microvilli. Around stage 62 the embryonic epithelium thickens and a massive cell death is observed in the epithelium, coinciding with eyelid opening. After metamorphosis, the frog cornea has attained the adult structure of three cellular layers, epithelium, stroma, and endothelium, and two acellular layers between the cellular layers, namely the Bowman's layer and Descemet's membrane. After initial completion, *Xenopus* cornea, in particular the stroma, continues to thicken and enlarge throughout the lifetime of the animal. In the adult, a p63 positive limbus-like wavy structure is observed at the peripheral edge of the cornea. Proliferation analysis shows that the basal corneal epithelial cells actively divide and there are a small number of proliferating cells among the stroma and endothelial cells. This study shows that the development and structure of *Xenopus* cornea is largely conserved with human although there are some unique processes in *Xenopus*.

1. Introduction

The cornea, as the anterior-most part of the eye, directly interacts with the external environment. It maximizes light transmittance into the eye and, with an even higher refractive power than lens, accounts for 70–75% of the eye's total refractive power. In addition, the cornea functions as a physical barrier to protect deep ocular structures from potentially harmful organisms and substances. The cornea meets these critical roles by employing a unique complex three-layered structure comprising a corneal epithelium layer, a stromal layer, and an endothelium layer without any pigmentation or vasculature. As one of the most sensitive tissues of the body, the cornea is also densely innervated with sensory nerve fibers. Studies of formation of the cornea, mainly using mammals and chick, have revealed complex mechanisms of corneal development and maturation (Linsenmayer et al., 1998; Soules and Link, 2005; Zhao et al., 2006; Zieske, 2004). Briefly, the vertebrate cornea begins its development as simple ectoderm tissue, which proliferates extensively under external signals to give rise to the primitive lens. Almost immediately after lens detachment, waves of neural crest cells (NCCs) migrate into the space between lens and epithelium. In chick, it is believed that neural crest invasion occurs in two steps. The first wave develops into corneal endothelium, followed by the second wave, which differentiates into keratocytes.

Abbreviations: NCC, neural crest cell; SAC, stroma-attracting center; CMZ, ciliary marginal zone.

* Corresponding author. Tel.: +44 20 7608 4062.
E-mail address: s.ohnuma@ucl.ac.uk (S.-i. Ohnuma).

[1] These authors contributed equally to this work.

0014-4835/$ – see front matter © 2013 The Authors. Published by Elsevier Ltd. All rights reserved.
http://dx.doi.org/10.1016/j.exer.2013.07.021

In contrast, studies in rodents described a single migration of cells giving rise to both cell types. In addition, a recent report (Gage et al., 2005) provided evidence that in mouse, keratocytes and endothelial cells are derived from a mixture of NCCs and head mesoderm.

Defects of corneal development or maintenance are a major cause of blindness. Also, slight changes in corneal properties such as contour, smoothness, thickness, transparency or architecture result in visual distortion and loss of clarity. Recently, many genes that are associated with corneal diseases have been identified (Aldave, 2011; Nielsen et al., 2013; Schmedt et al., 2012). Human corneal diseases often manifest their associated defects in specific layers of the cornea. For example, Meesmann's juvenile dystrophy manifests as a defect in the corneal epithelium, while granular dystrophy and Fuchs' dystrophy manifest as defects in the stroma and endothelium layers respectively. Some diseases are in contrast associated with multiple layers. Interaction between the layers is likely to play a critical role in corneal pathogenesis. However, an understanding of the molecular interactions underlying disease pathology, necessary for prevention of disease and the development of novel treatments, is at present almost entirely lacking. This is largely due to a lack of suitable assay models. There is no good *in vitro* model of this three-dimensional complex structure of epithelium, stroma, and endothelium. Also, mammalian models are limited (Koizumi et al., 2012; Stuart and Keadle, 2012) and are not ideal for the investigation of detailed mechanisms because of the cost, time and limits on animal number. Therefore, development of suitable animal models using more accessible lower animals are required in order to gain better understanding of the pathogenesis of human corneal diseases.

The African clawed frog, *Xenopus laevis/tropicalis*, has been used extensively as a model organism. Its rapid development and ease of manipulation have made it particularly suitable for studying some complicated developmental processes. Recently, a new technology of gene knockout, transcription activator-like effector nucleases (TALENs) (Mussolino and Cathomen, 2012), has proved to be effective in *Xenopus* (Ishibashi et al., 2012; Lei et al., 2012). This technology was developed by genetic engineering of bacterial proteins, transcriptional activator-like effectors, which recognize specific nucleotide sequences (Boch and Bonas, 2010). Simple injection of two engineered TALENs into *Xenopus* blastomeres results in gene knockout with almost 100% efficiency in the F0 embryos, which can produce a further generation. The F1 frogs can produce a few thousand in the next generation, indicating that *Xenopus* may be an ideal organism to construct corneal disease models.

Despite extensive studies on lens regeneration using *Xenopus* cornea (Filoni, 2009; Henry and Tsonis, 2010), our knowledge of its structure and formation is very limited. In 1979, Bard and Abbott briefly described its development. They found that at stage 32, periocular mesenchymal cells start to migrate into the space between the corneal epithelium and the lens to form the monolayer structure of the prospective endothelium, connected to the outer cornea in the center. Around stage 43, additional mesenchymal cells were observed to colonise the space between the two corneal layers. By stage 63, outer cornea and inner cornea are completely joined with corneal stroma in between (Bard and Abbott, 1979).

In human, cornea formation is largely complete at 5 months gestation. At birth, all components of the cornea are already present in their proper proportions. After the fetal period, the cornea maintains its structure without significant changes in thickness, as the human eye does not change much in size during its lifetime. However, amphibian and fish eyes grow during the whole life of the animal. Reflecting this, adult amphibian and fish have functional retinal stem cells in the peripheral retina, called the ciliary marginal zone, which continue to produce retinal neurons and glial cells (Ohnuma et al., 2002). It is known that the human cornea has limbal stem cells at the periphery, which contribute to the maintenance and repair of the cornea. However, nothing is known about *Xenopus* corneal stem cells.

Metamorphosis, a unique feature of the amphibian lifecycle, adds more complexity to this process. *X. laevis* tadpoles start metamorphosis at stage 48 through activation of thyroid hormone (Nieuwkoop and Faber, 1967). They first develop hind limbs and fore limbs, followed by gradual degeneration of the tail. All processes are complete by stage 66. Along with changes in external appearance, the structures and functions of many internal organs are also altered to be better suited for a new lifestyle and living environment, such as a functional lung that develops to breathe air directly (Pronych and Wassersug, 1994). Dramatic changes also occur in the eye. Before metamorphosis, all retinal ganglion cell axons project to the contralateral tectum in the diencephalon. However, during metamorphosis, they start to project to the ipsilateral side, providing a wider view to cover both front and lateral sides, which is advantageous for catching prey while remaining aware of the surrounding environment (Nakagawa et al., 2000). So far, nothing is known about changes of the *Xenopus* cornea during metamorphosis.

Therefore, this paper investigates details of *Xenopus* corneal development, including embryonic cornea formation, the changes that occur during metamorphosis, the maturation process and the structure of the adult frog cornea. It clearly reveals the potential of using the *Xenopus* cornea as a new system to investigate the detailed molecular mechanisms of human corneal disorders.

2. Experimental procedures

2.1. Xenopus eye tissue processing

Xenopus embryos were obtained by *in vitro* fertilization, and staged according to Niewkoop and Faber (Nieuwkoop and Faber, 1967). Prior to processing, embryos younger than stage 45 were anaesthetised by immersion in 0.1× Modified Barth's Saline (MBS) containing 0.2 mg/ml tricaine methanesulfonate (MS222). Tadpoles staged between 50 and 66 were immersed in MS222 at a concentration ranging from 0.5 to 2 mg/ml. Older and bigger tadpoles require a higher dosage of MS222 for full anaesthetisation. Adult *Xenopus* frogs were anaesthetised by injecting 600 μl of 0.4 g/ml MS222. For *Xenopus* older than stage 50, the tadpoles were decapitated and only heads were processed. In the case of adult frogs, eyes were carefully dissected out and processed.

2.2. Electron microscopy (EM)

Tissues were embedded in epoxy resin for examination by both light and electron microscopes. Tissues were fixed in Karnovsky fixative comprising 3% (v/v) glutaraldehyde, 1% (v/v) paraformaldehyde in 0.08 M sodium cacodylate pH 7.4, followed by secondary fixative 1% (w/v) osmium tetroxide for 2 h. Following osmication, tissues were rinsed in distilled water and then passed through ascending alcohols: 50%, 70%, 90%, 100% for 10–15 min. After ethanol dehydration tissues were passed via propylene oxide (epoxy propane) then a 1:1 mixture of propylene oxide and Araldite to 3–6 h in full resin. Samples were embedded in fresh resin, labeled and placed in a 60 °C oven overnight to polymerize as reported (Coulter, 1967).

After polymerization, the resin was trimmed away from the tissue surface using a Reichert Jung OM-3 ultra-microtome. For light microscopy, thick sections (1 μm) were cut by diamond knife and collected on a glass slide. For EM, thin sections (70–90 nm) were cut and picked up onto mesh grids.

Sections for light microscopy were stained with toluidine blue. Eyes were viewed using a Zeiss Axioskop2 plus microscope and images were taken using Q Capture software. Grids for EM were stained with lead citrate. Ultrathin sections were viewed on a JEOL1010 transmission electron microscope (TEM) and digital images were taken using Gatan micrograph software.

2.3. Ultrastructural analysis using serial block-face scanning electron microscopy with Gatan 3View

For 3D view analysis tissue fixed in 3% glutaraldehyde and 1% paraformaldehyde buffered to pH 7.4 with sodium cacodylate was rinsed in buffer, then incubated in a solution containing 3% potassium ferrocyanide, 0.3 M cacodylate buffer, 4 mM calcium chloride with an equal volume of 2% osmium tetroxide, and then placed in the filtered thiocarbohydrazide solution and en bloc stained with uranyl acetate and Waltons lead citrate using the previously reported method (West et al., 2010).

The specimen embedded in epoxy resin by conventional TEM methods was placed in an automated serial sectioning device (Gatan 3-view system) located within the specimen chamber of the Zeiss Sigma FESEM providing 3- dimensional data. Using the system, carefully trimmed block faces measuring 0.2 × 0.2 mm were sectioned with a diamond knife in increments of as little as 40 nm. The block face was then scanned in backscatter mode and the Z-contrast component used to form a TEM-like image of the specimen, before another section was cut and imaged. Cutting was repeated over 1000 increments during an overnight run. The system generated a large volume of digital data that could then be played back to give 3D-view images with nanometer resolution (Denk and Horstmann, 2004).

2.4. EdU labeling for proliferative cells

EdU (5-ethynyl-2′-deoxyuridine, Invitrogen Cat. No. C10337) was used to label proliferating cells in *Xenopus* embryos. A 1 mM concentration of EdU was made with sterile phosphate buffered saline (PBS). Embryos were anaesthetised in 0.1× MBS with 0.2 mg/ml MS222 and placed belly-up in plates with plasticine beds. For embryos younger than stage 40, 30 nl of EdU solution was injected into the cranial space between the developing eyes. For embryos between stage 40 and 45, 30 nl of EdU solution was injected subcutaneously in the abdominal area of the embryos. Injection dosages for older animals are: Stage 50, 5 μl of 2.5 mg/ml EdU solution; Stage 60, 62 and 65, 40 μl of 2.5 mg/ml EdU solution; two-year-old adults, 2.5 ml of 2.5 mg/ml Edu solution. After injection, embryos and tadpoles were cultured for a period of time specified by the experiment (1.5, 3 and 12 h) and then fixed with 4% paraformaldehyde (PFA) and processed for cryosectioning or paraffin sectioning. Sections were processed to visualize the EdU signals according to the manufacture's protocol (Molecular Probes Invitrogen Edu Imaging Kits). Processed sections were viewed using Zeiss Axioskop2 plus microscope and images were acquired using Q-Capture software.

2.5. Tissue processing for cryosections

Samples were fixed in 4% PFA in PBS for 1 h at room temperature. After fixation, the samples were maintained in 30% sucrose in PBS until samples had sunk to the bottom. Sucrose was then replaced by Optimal Cutting Temperature (OCT) compound. After OCT had set, the sample blocks were stored at −80 °C. Sections were made at 10 μm thickness using a cryostat (Leica) and collected on glass slides. Sections were processed to visualize the EdU signals according to the manufacture's protocol (Molecular Probes Invitrogen Edu Imaging Kits).

2.6. Tissue processing for paraffin sections

Xenopus samples were prepared and fixed in 4% PFA in PBS. After fixation, PFA was replaced by ethanol and the samples were passed through two changes of xylene before transfer to 58 °C molten wax. Tissue sections were made at 7–10 μm thickness on a microtome, and collected on glass slides, sections were then dewaxed before further processing. Sections were processed to visualize the EdU signals according to the manufacture's protocol (Molecular Probes Invitrogen Edu Imaging Kits). Sections were viewed using a Zeiss Axioskop2 plus light microscope.

2.7. Transplantation of neural crest precursor tissue

In order to label tissue for grafting, fluorescent dextran (Molecular Probes) was injected into both blastomeres of donor embryos at the 2-cell stage. At stage 18, the vitelline membrane of donor embryos and stage-matched recipient embryos was removed in 0.1× MBS approximately one hour prior to grafting. The donor embryo was placed in 1× MBS solution, lying on one side and secured in placed by surrounding plasticine. The surface epidermis was peeled away by an eyebrow knife. Gentle brushing parallel to the embryo surface towards the neural tube with the eyebrow knife removed the loosely attached cranial neural crest tissue. The donor neural crest was transplanted to an unlabeled embryo whose corresponding cranial neural crest had already been removed, keeping the anteroposterior orientation of the neural crest unchanged. To help with the healing, a small piece of broken glass coverslip was gently pressed down on the graft and removed after 20 min. After transplantation, embryos were cultured in 0.5× MBS supplemented with 0.1% gentamycin until stage 34 and 0.1× MBS afterward.

Grafted embryos were imaged using a Leica microscope.

2.8. DiI labeling of the cranial neural crest tissue

DiI (1,1′-dioctadecyl-3,3,3′,3′-tetramethylindocarbocyanine perchlorate, from Molecular Probes) was reconstituted in ethanol at 2 mg/ml and stored at −20 °C. Labeling was done on stage 15 embryos which had their vitelline membrane removed one hour prior to labeling. Embryos were secured in place by plasticine in 1× MBS solution. Injection mixture was prepared (10% DiI, 10% sucrose in water) and injected into the cranial neural crest tissue. After 15 min of healing, embryos were transferred to 0.5× MBS supplemented with 0.1% gentamycin in order to avoid fungal and bacterial contamination. After stage 34, embryos were cultured in 0.1× MBS. Grafted embryos were imaged using a Leica microscope.

2.9. Immunostaining using p63 antibody

After three 10 min washes in PBST (0.2% Triton X-100 in 1× PBS), sections were blocked in blocking buffer (5% goat serum (Sigma), 0.2% Triton X-100, 0.2% BSA in 1× PBS) for 30 min at RT, followed by p63 primary antibody (Santa Cruz, sc-8431) incubation at 4 °C overnight. On the second day, sections were washed three times in PBST for 10 min each time and then incubated with anti-mouse IgG at RT for 60 min, protected from light. Three 15 min washes in PBST were performed to remove the unbound antibodies and sections were mounted in FluorSave™ reagent (Calbiochem).

3. Results

3.1. Stage 25 − eye vesicle formation

At this early stage of eye morphogenesis, the optic cup is formed of the eye vesicle, which is derived from evagination of the neural

tube, covered by fully differentiated embryonic epidermis. The embryonic epidermis has a distinctive layered structure. The cornea at this stage – the ectoderm tissue – comprises two layers (Fig. 1A, B, C), an apical embryonic epidermis layer containing goblet cells and ciliated cells (Fig. 1G–I) together with a basal embryonic epidermis layer, which receives signals from the developing retina to proliferate and produce lens. In goblet cells (Fig. 1H), mucus-secreting vesicles form on the apical membrane, underneath which a large number of mitochondria can be observed (Fig. 1H arrow heads). In addition, numerous electron-dense platelets are seen in all cells (Fig. 1G). These might be nutrient rich yolk platelets supplying energy and resources for the embryos. EdU labeling reveals, in addition to extensive division of retinal precursors, occasional dividing cells in the basal corneal epidermis but no division in the apical corneal epidermis (Fig. 1D, E, F), suggesting that the basal cells are dividing very slowly while the apical embryonic epidermal cells are not actively proliferating. At this stage, the cells in the retina facing the epidermis start to be determined as retinal ganglion cells. This is the first retinal cell fate determination (Kanekar et al., 1997).

3.2. Stage 30 – lens induction from the cells

Under the induction signals secreted by the developing retina, cells in the center of the basal epidermal layer undergo active proliferation to give rise to presumptive lens cells, as evidenced by EdU labeled cells at the junction of basal epidermis and lens (Fig. 1J–L, N–P). Most of the lens cells have exited the cell cycle. The basal epidermis and lens are still connected at this stage (Fig. 1L, R, S). This process of lens induction has been well studied and these studies demonstrated that the embryonic lens is derived from early stage cornea (Day and Beck, 2011; Walter et al., 2004). Periocular mesenchymal cells have migrated into the space between retina and embryonic epidermis (Fig. 1M). These cells will form the inner cornea/endothelium. An enlarged intercellular space, which does not have fully formed intercellular junctions, is established between the ectodermal cells (Fig. 1Q). The fate of most of the retinal ganglion cells has been determined and some photoreceptor cells have begun to be determined in the retina, which therefore, shows a vaguely layered structure (Fig. 1K).

3.3. Stage 35 – lens detachment and anterior chamber formation

At this stage, the lens has detached from the basal epidermis and periocular mesenchymal cells have migrated further in to occupy the space between lens and epidermis (Fig. 2A–C). These mesenchymal cells are loosely associated with each other and form an imperfect layer. In places, they are observed stacking on top of each other (Fig. 2C and H). In addition, a thin matrix is found developing between the basal epidermis cells and the mesenchymal cells (Fig. 2G and I), possibly secreted by the basal epidermis cells where numerous mitochondria and large networks of rough endoplasmic reticulum (ER) are observed (Fig. 2K). In embryonic chick cornea, the epithelial cells secrete a collagenous matrix, termed the primary stroma, prior to the influx of neural crest cells (NCCs) (Pinnamaneni and Funderburgh, 2012). This primary stroma is not observed in rabbits, mice or primates. Interestingly, cross-sections of processes, possibly from the mesenchymal cells, can be seen in the matrix (Fig. 2J). As such cellular processes were not observed in any later stages examined in this study, they are possibly transitional structures that the mesenchymal cells rely on for migration and positioning during the establishment of the monolayer.

3.4. Stage 37–39 – initiation of the corneal endothelium

The mesenchymal cells are lined up in an imperfect monolayer, and the intercellular connections are not yet fully established (Fig. 3A, B, C). As this monolayer will eventually develop into the corneal endothelium, we propose to name it presumptive corneal endothelium. At the peripheral region of the cornea where it attaches to the peripheral retina, developing blood vessels, possibly the episcleral vasculature, were always observed (Fig. 3B, D). The vasculature is located just outside the ciliary marginal zone (CMZ) of the retina, which contains retinal stem cells at the most peripheral edge. The importance of an association of neural stem cells with vasculature has been reported (Goldberg and Hirschi, 2009), suggesting that the vasculature observed here might be important for maintenance and functioning of the retinal stem cells. At this stage, the detached lens has started differentiation and the three layers of retinal ganglion cell layer, interplexiform cell layer, and photoreceptor cells were observed. EM images show that the apical embryonic epidermis layer is still formed of ciliated cells and goblet cells (Fig. 3I). Ciliated cells are sparsely distributed among goblet cells. Ciliated cells are significantly fewer in number than goblet cells and can be identified by the cilia on their surface and by the darker staining they exhibit in both EM and semi-thin sections. Ciliated cells are found on the anterior corneal surface of humans (Lohman et al., 1982; Pfister, 1983), some species of monkeys (Pfister, 1983), and other mammals including cat, dog, rat (Pfister, 1983) and rabbit (Doughty, 1990). These microprojections increase the cell surface area and improve the absorbance of oxygen and nutrients as well as the movement of metabolic products across the outer cell membranes. In human and other mammals the epithelial surface of the cornea is naturally hydrophobic. Therefore, for a tear layer to be able to remain on the corneal surface without rolling off, the hydrophilic mucoid or mucin layer of the tear film is laid down onto the surface of the cornea by goblet cells (Dohlman, 1971). Intercellular junctions start to develop among the corneal epidermal cells (Fig. 3H, K–N). The matrix subjacent to the epidermis is thicker compared to stage 35 (Fig. 3 J). Mitochondria and rough ER are frequently found in the presumptive corneal endothelial cells indicating their active status (Fig. 3 J′). EdU staining reveals proliferating cells in all corneal layers at this stage (Fig. 3 E, F, G, arrows in insets) as well as in the episcleral vasculature (arrowheads).

3.5. Stage 41 – second stream of cell migration contributes to cornea formation

At this stage, the cornea arches out to create an anterior chamber between cornea and lens. The smooth and continuous presumptive corneal endothelium is completely separated from the embryonic epidermis except in the center, where they are connected by a small number of cells (Fig. 4A–C). This unique structure has been reported in previous studies (Bard and Abbott, 1979). Sections further away from the center revealed more clearly that a second stream of cell migration is taking place, invading the matrix between the epidermis and the presumptive endothelium (Fig. 4D–E). While all corneal layers are stacked together at the center (Fig. 4I), in more peripheral regions, segregation of the cornea layers results in the formation of presumptive outer cornea and presumptive inner cornea (Fig. 4J). The migrating cells are flat fibroblast-like cells with long cellular processes and a high nuclear to cytoplasmic ratio (Fig. 4N–P). They will later contribute to the formation of outer and inner corneas and likely differentiate into keratocytes in the mature cornea. Tight junctions (Fig. 4K) and desmosomes (Fig. 4K–M) can be clearly identified in the epidermis, but not in the presumptive corneal endothelium (Fig. 4Q). Corneal cells are still actively dividing as seen by the EdU labeling (Fig. 4F–H).

3.6. Stage 43–45 – clear separation between the embryonic inner cornea and outer cornea

At this stage, the space between cornea and lens has become much smaller compared to earlier stages, and the limited space in

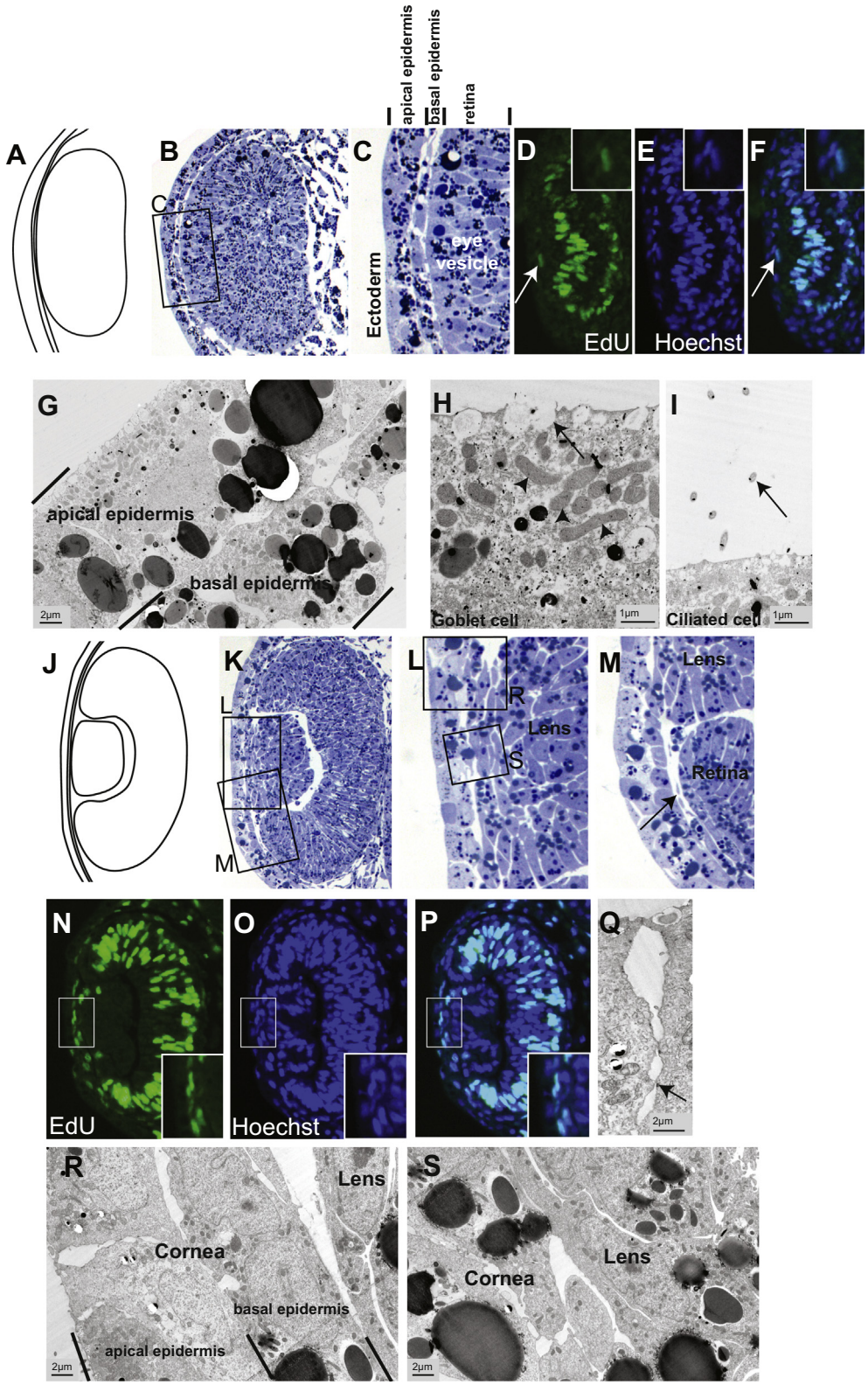

Fig. 1. *Xenopus* cornea at stage 25 and stage 30. (A) Schematic drawing of a stage 25 eye. (B–C) Plastic section images of stage 25 eye (B) and the epidermis overlying the developing retina at this stage (C). (D–F) Proliferation assay of stage 25 cornea. EdU (D), Hoechst (E), and overlaid (F). Arrow indicates a dividing cell in the basal corneal epidermis overlying the optic cup. (G–I) EM image showing the two-layered structure of the epidermis in the stage 25 cornea. The apical epidermis consists of goblet cells (H) and ciliated cells (I). (H) shows that mucus secreting vesicles (arrow) form on the apical plasma membrane in a typical goblet cell and numerous mitochondria (arrowheads) close to the cell membrane indicate the active status of the cell. Ciliated cells (I) possess long cilia on the apical membrane, the cross-section of which is indicated by an arrow here. (J) Schematic drawing of stage 30 eye. (K–M) Plastic section images of stage 30 eye (K), cornea (L) and the periocular region (M). Mesenchyme (arrow in M) migration is observed in the periocular space. (N–P) Proliferation assay of stage 30 cornea showing the actively dividing basal epidermal cells in the cornea. EdU (N), Hoechst (O), and overlaid (P). (Q) Intercellular junctional complexes are not fully formed (arrow) at this stage. (R, S) EM images of a plastic section adjacent to that displayed in panels K–M. (R) Epidermis in the cornea retains its two-layered structure, (S) the basal epidermis cells closely associate with the presumptive lens cells.

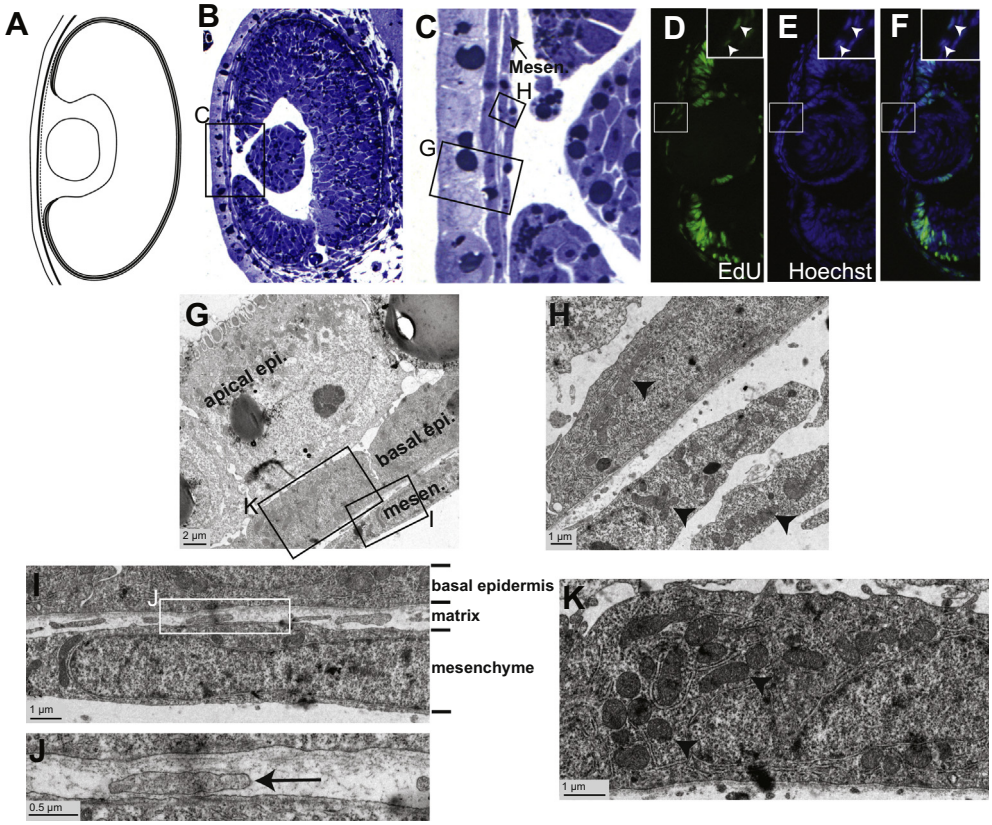

Fig. 2. *Xenopus* cornea at stage 35. (A) Schematic drawing of stage 35 eye. (B–C) Plastic section images of stage 35 eye (B) and cornea (C). Mesenchyme (arrow in C) is found lining the entire length of the basal epidermis. (D–F) Proliferation assay showing dividing cells in the epidermis (arrowheads in insets). EdU (D), Hoechst (E), and overlaid (F). (G–K) EM images of a plastic section adjacent to that displayed in panels B and C showing that the cornea at this stage is composed of two epidermis layers, a thin matrix and some mesenchymal cells. (G) The mesenchymal cells have not yet formed a monolayer (H) and their high cellular activity is suggested by the presence of many mitochondria (arrowheads) in the cytoplasm. (I–J) High magnification EM images showing the thin matrix in the cornea (I), where cross-sections of mesenchymal cell processes (J) are observed. (K) Basal epidermis cell shows dark staining in EM and cellular organelles such as ER and mitochondria (arrowheads) are abundant in their cytoplasm. Abbreviations: mesen, mesenchyme; apical epi, apical epithelium; basal epi, basal epithelium.

between is filled with a light-staining matrix (Fig. 5A–C). The fibroblast-like presumptive keratocytes segregate, resulting in the formation of outer cornea and inner cornea, joined only at the center (Fig. 5A, B, C, G and Q). Both the outer and inner corneas are multilayered structure (Fig. 5G). The outer cornea comprises four layers (Fig. 5H), apical and basal embryonic epidermis, matrix and presumptive keratocytes. The outermost layer, the apical embryonic epidermis, is made of mucus-secreting goblet cells (Fig. 5J) and ciliated cells. These cells contain a large number of mitochondria just under the apical plasma membrane (Fig. 5K, L). The second layer comprises more darkly stained basal epidermis cells, which contain an extensive network of rough ER (Fig. 5M) and are possibly responsible for synthesizing the matrix lying underneath (Fig. 5O). Between the epidermal cells, well-established intercellular connections such as tight junctions and desmosomes were found (Fig. 5I). Active communication was observed at the interface between these two layers of cells (Fig. 5N). The fourth layer of the outer cornea and the outermost layer of the inner cornea are likely both derived from the second wave of migrating cells. They are both large and flat in appearance. Rough ERs and mitochondria could sometimes be observed in their cytoplasm (Fig. 5O, P). The inner cornea comprises presumptive keratocytes and presumptive corneal endothelium together with the matrix sandwiched between them (Fig. 5P). The cell mass that connects the outer and inner corneas comprises less than 10 cuboidal shaped cells covered by a thin matrix, which joins to the matrices in the outer and inner corneas (Fig. 5Q–S). The cell bodies attach anteriorly to the basal epidermis cells but are separated by a thin layer of matrix from cells of the inner cornea/presumptive corneal endothelium (Fig. 5C). Therefore, we speculate that they might be derived from embryonic epidermal cells in the outer cornea. Dividing cells were observed in the cornea at this stage according to the proliferation assay results (Fig. 5D–F).

At this stage the iris becomes apparent, formed of two layers of pigmented and non-pigmented epithelia. The inner cornea connects with the sclera at the iridocorneal angle (Fig. 5B). In the angle, we could observe endothelial cells lining the annular ligament. At this stage, all the layers in the central neural retina have differentiated and are fully functional. We could observe the CMZ at the edge of the retina with retinal stem cells at the peripheral end of the CMZ. The retinal stem cells will continue to divide (Fig. 5D–F) and produce neurons and glial cells throughout the life of the animal (Perron et al., 1998).

3.7. Origin of the inner cornea

It is well established that the cornea is formed of cells that are of epidermis (ectoderm), neural crest (ectoderm) and in some cases mesodermal origins. In mouse, it was shown that the corneal epithelium originates from embryonic ectoderm/epidermis, while stroma as well as endothelium contain a mixed population of neural crest tissue and head mesoderm tissue (Zhao et al., 2006). In contrast, chick corneal stroma and endothelium contain solely cells of neural crest origin (Boch and Bonas, 2010; Ishibashi et al., 2012; Mussolino

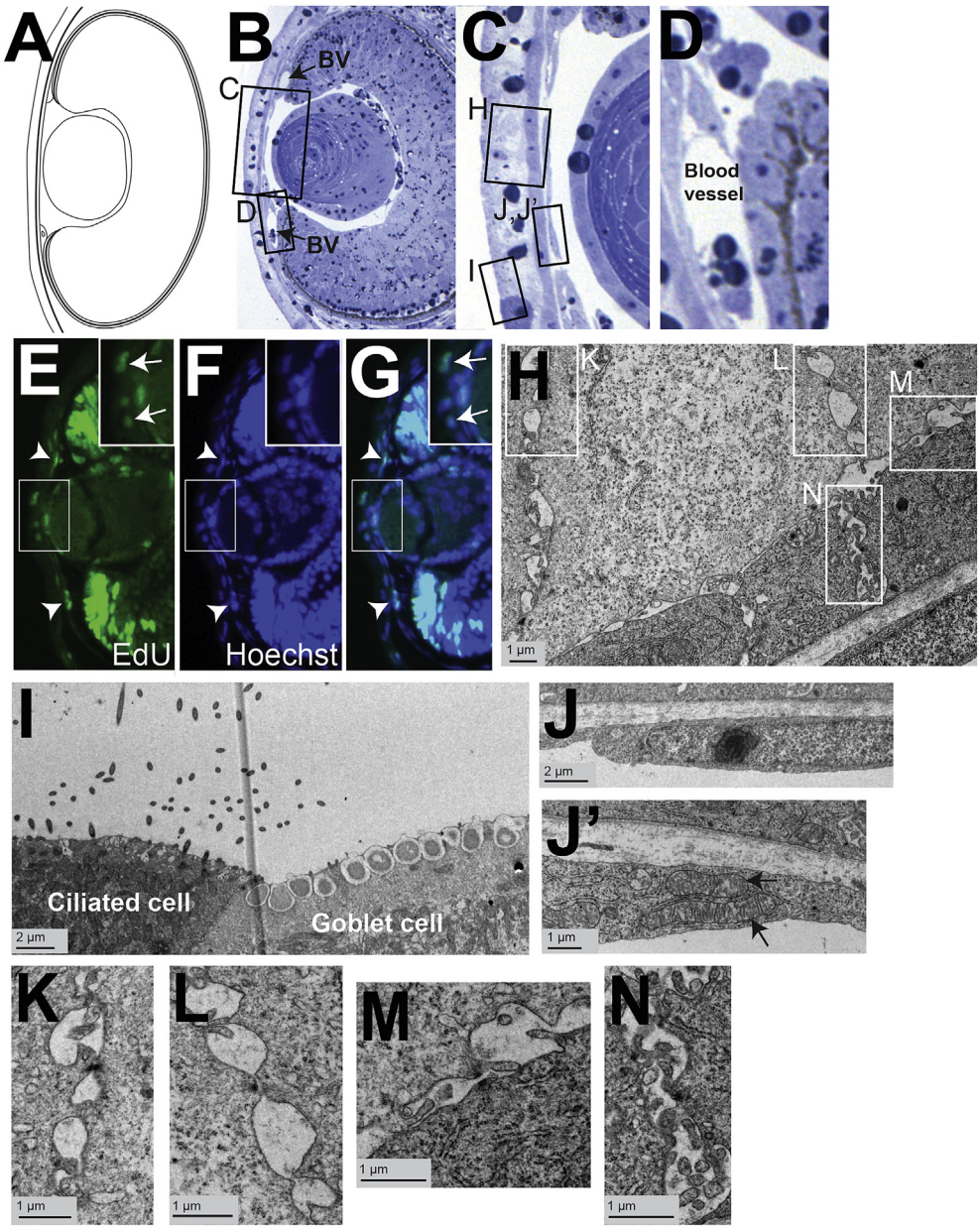

Fig. 3. *Xenopus* cornea at stages 37–39. (A) Schematic drawing of stage 37–39 eye. (B–D) Plastic section image of stage 37–39 eye (B), cornea (C) and the developing episcleral vasculature (D). (E–G) Proliferation assay showing positively labeled cells in the cornea (arrows in insets) as well as in the developing vasculature (arrowheads). EdU (E), Hoechst (F), and overlaid (G). (H–N) EM images of a plastic section adjacent to that displayed in panels B–D showing details in the stage 37–39 cornea. The cornea is composed of four distinct layers (H) at this stage. The cornea anterior surface is formed by goblet cells and more darkly stained ciliated cells (I). The matrix layer appears thicker than at earlier stages (J, J′) and the mesenchymal cells are arranged into a monolayer named the presumptive corneal endothelium. Organelles such as mitochondria (arrows) are sometimes observed in the cytoplasm. (K–N) High magnification images of the developing intercellular connections in the cornea epidermis. Abbreviations: BV, blood vessel.

and Cathomen, 2012; Soules and Link, 2005). In order to understand the contribution of NCCs and surface ectoderm in the formation of the *Xenopus* cornea, we took cranial neural crest tissue from fluorescein dextran labeled donor embryos and grafted it to the corresponding area on an unlabeled recipient at stage 20 (Fig. 6A). The graft tissue integrated well into the host embryos and migrated in three streams as seen at stage 26 (Fig. 6B, C, D) and later gave rise to the cartilaginous structures in the head (Fig. 6E). At stage 45, the entire inner cornea was labeled (Fig. 6F, G, H) whereas the outer cornea was not, suggestive of the neural crest origin of the inner cornea and epidermis origin of the outer cornea. Consistent with this observation, the side of the donor embryo with NCC removed failed to develop an inner cornea (Fig. 6I) while the inner cornea on the control side developed normally (Fig. 6J). In order to confirm this is not an artifact caused by transplantation, we labeled the mandibular neural crest segment with DiI at stage 15 (Fig. 6K). The labeled cells developed into periocular mesenchyme at stage 26 (Fig. 6L) and the inner but not outer cornea at stage 45 (Fig. 6M, N, O, P).

3.8. Stage 48–50 – active stromal cell migration toward the stroma attracting center

The central inner cornea remains closely attached to the lens (Fig. 7A–D). Changes occur to the multilayered structure of both outer and inner corneas. The presumptive keratocyte cells previously lining the outer cornea and inner cornea have dispersed and

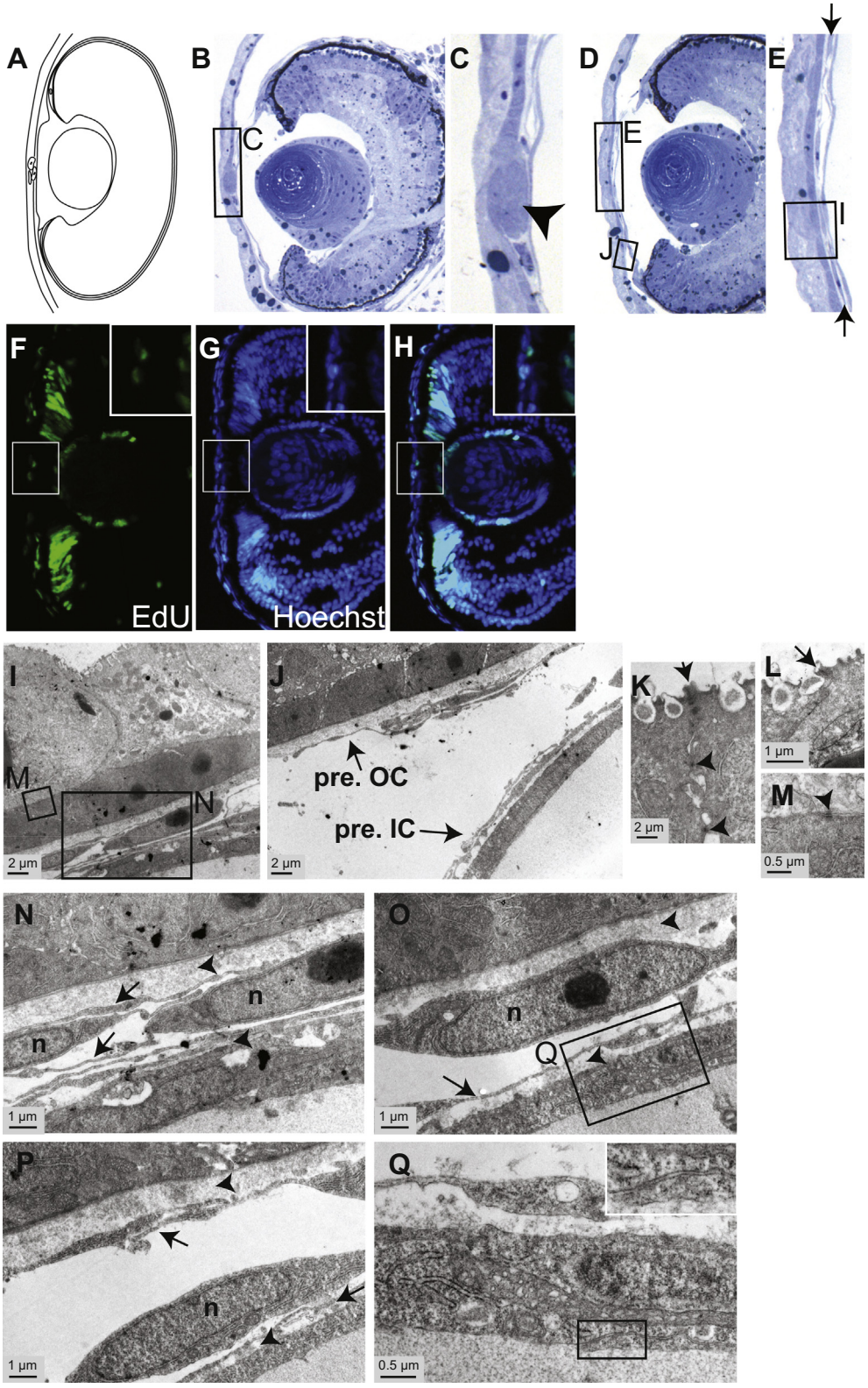

Fig. 4. *Xenopus* cornea at stage 41. (A) Schematic drawing of stage 41 eye. (B–E) Plastic section image of stage 41 eye (B, D) and cornea (C, E). Embryonic epidermis and endothelium associate via a small group of cells in the central cornea (arrowhead in C). The second migratory wave is seen invading the matrix as indicated by arrows in (E). (F–H) Proliferation assay. EdU (F), Hoechst (G), and overlaid (H). (I–Q) EM images of a plastic section adjacent to that displayed in panels D and E. (I) EM image showing structure at the center of the cornea. (J) At the periphery, segregation of presumptive outer cornea and inner cornea (arrows) is observed. (K–M) Tight junctions (arrows) and desmosomes (arrowheads) are observed between two goblet cells (K), between one goblet cells and one ciliated cell (L), and between one apical epidermal cell and one basal epidermal cell (M). (N–P) EM images showing the second wave of migrating mesenchymal cells, with N being closest to central cornea and P being closest to peripheral cornea. The migrating mesenchymal cells have big nuclei (n) with thin and long cell processes, shown by arrows. The primary matrix is invaded by mesenchyme and split up into two parts, indicated by arrowheads. (Q) High magnification image showing the cellular contents and the absence of intercellular junctions between two presumptive corneal endothelial cells (inset). Abbreviations: pre. OC, presumptive outer cornea; pre. IC, presumptive inner cornea; n, nucleus.

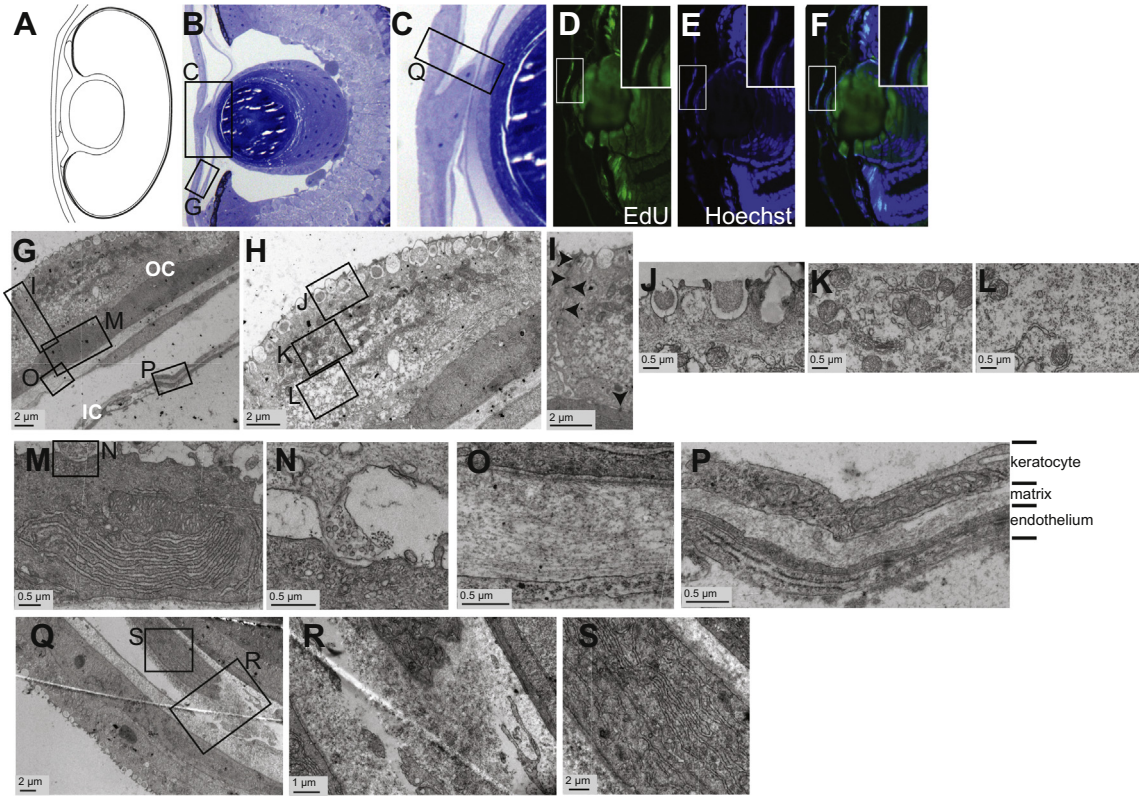

Fig. 5. *Xenopus* cornea at stages 43–45. (A) Schematic drawing of stage 43–45 eye. (B–C) Plastic section images of stage 43–45 eye (B) and cornea (C). (D–F) Proliferation assay. EdU (D), Hoechst (E), and overlaid (F). (G–S) EM images of a plastic section adjacent to that displayed in panels B and C. (G) EM image showing the multiple layered structures of the outer cornea and inner cornea. (H) The outer cornea comprises four layers. (I) Mature intercellular junctions are identified between epidermal cells, indicated by arrowheads. (J–L) High magnification images of the cellular contents of a goblet cell in apical to basal order. (M) A typical basal epidermal cell contains extensive ER in the cytoplasm. (N) Active communication observed between apical and basal epidermal cells. (O–P) EM images of the matrix and presumptive keratocyte layer of the outer cornea (O), and the structure of the inner cornea (P). (Q–S) The central connection is composed of cuboidal cells (S) surrounded by a matrix material (R). Abbreviations: OC, outer cornea; IC, inner cornea.

are found in the space between outer cornea and inner cornea (Fig. 7C, E, G). The connection between inner cornea and outer cornea persists and now consists of around 20 cells (Fig. 7D). We propose to call this the stroma-attracting center (SAC) because stroma keratocytes are mainly distributed close to this connection structure (Fig. 7C, D, G). Cells of the outer cornea are undergoing significant changes (Fig. 7E, F). The previous four-layered structure no longer exists (Fig. 7N). The ectodermal derived cells are no longer arranged in an orderly manner in perfect layers, but instead, are located rather haphazardly (Fig. 7E, F), and the mucus-secreting vesicles are replaced with some microvilli and vesicular structures on the apical plasma membrane (Fig. 7O). The cells have both microvilli and secreting vesicles, suggesting that they are transitional epithelial cells. Numerous dark stained particles can be observed underneath the epithelial cells (Fig. 7P). The previously layered inner cornea is transformed into just a single cell layer of presumptive corneal endothelium (Fig. 7W). Interestingly, some fish-bone like collagen fibrils are observed close to both epithelium and endothelium (Fig. 7N, P, W). Therefore it seems that collagen fibril construction and assembly occur in an edge to center manner. The stromal cells contain rough ER (Fig. 7R and V) and small vesicles (Fig. 7U) in their extending processes. Inside some relatively big intracellular vesicles, short collagen fibrils measured at approximately 0.1 μm in length were observed (Fig. 7S, T), suggesting that the complex collagen assembly process might start inside the keratocytes. Furthermore, a thin layer of matrix was observed adjacent to the cells in the SAC as well (Fig. 7X, arrowhead in Fig. 7Y). Cells in the epithelium and in the SAC are both dividing at this stage, as evidenced by the EdU staining (Fig. 7H–M). We hardly observed any EdU-labeled keratocytes, implying that any potential increase in keratocyte number in the stroma is due to cell migration from periocular space, rather than a result of proliferation of existing keratocytes.

The 3D structure of the SAC was investigated in detail using the 3View system. 1000 consecutive sections (10 nm) of *Xenopus* cornea, at stage 50, were examined by EM and the 3D structure was reconstructed using 3View software (Supplemental movie). Fig. 8A–G show selected sections of the SAC. These images clearly show that corneal epithelial cells are connected to the corneal endothelium via the SAC. At this stage, the SAC contains approximately 20 cells. The cell morphology and composition of intracellular organelles of the SAC cells are significantly different from those of the epithelial cells and endothelial cells. While around five apical SAC cells are in direct contact with the epithelial cells (Fig. 8C, D), basal SAC cells are completely separated from the corneal endothelium by some extracellular matrix (Fig. 8D–F). At this stage around ten migrating keratocytes are directly touching the SAC. Recently, NCCs have been shown to migrate together in a process known as collective migration (Carmona-Fontaine et al., 2008; Theveneau and Mayor, 2011). In contrast, these keratocyte cells seem to migrate individually as opposed to as part of a group.

Supplementary data related to this article can be found online at http://dx.doi.org/10.1016/j.exer.2013.07.021.

3.9. Stage 55–60 – mature corneal stroma starts to form

At stage 55, the cornea remains attached to the lens (Fig. 9A, B and R) by an obvious membrane-like dense structure between the

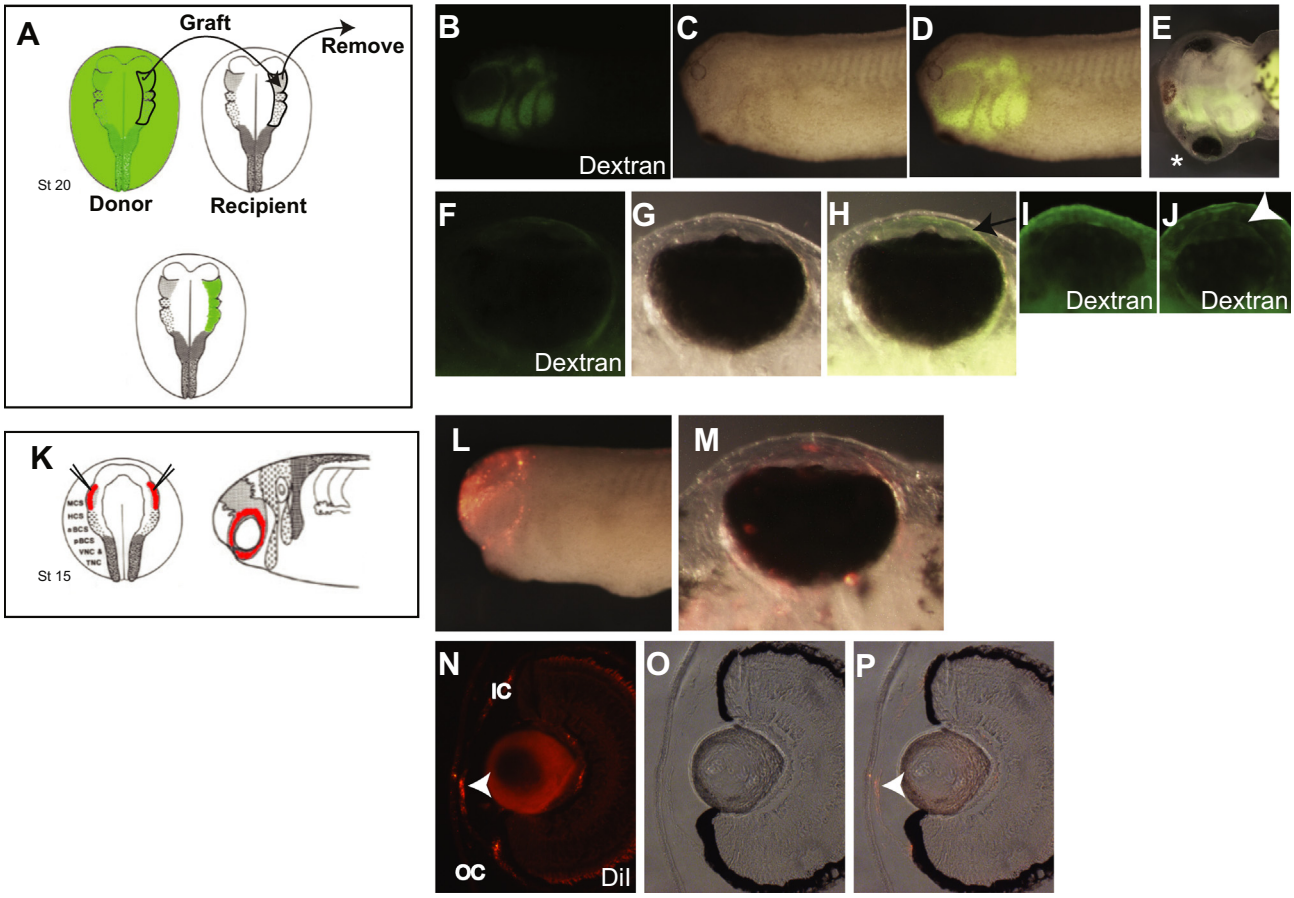

Fig. 6. NCCs contribute to the *Xenopus* cornea. (A) Schematic drawing of the labeled NCC grafting experiment. (B–D) Fluorescent (B), brightfield (C) and overlaid (D) images of a grafted embryo at stage 26 showing grafted tissue developing into three migrating streams of cranial neural crest. (E) Overlaid image of the ventral view of a grafted embryo at stage 45. Grafted side is labeled with an asterisk. (F–H) Fluorescent (F), brightfield (G) and overlaid (H) images of an eye at stage 45. The fluorescent inner cornea is indicated with an arrow. (I–J) Fluorescent images of the eyes of a donor embryo at stage 45. Image (I) shows the eye on the side where cranial NCCs had been removed. Image (J) shows the eye on the control side. Intact inner cornea is indicated with an arrowhead. (K) Schematic drawing of DiI labeling experiment. (L) Overlaid image of the labeled embryo at stage 26. (M) Overlaid image of the eye at stage 45. (N–P) Fluorescent (N), brightfield (O) and overlaid (P) images of the cross-section of a DiI labeled eye. Abbreviations: OC, outer cornea; IC, inner cornea.

lens and the corneal endothelium layer (arrow in Fig. 9R). The stroma-attracting center has disappeared. Primary corneal epithelium and endothelium are completely separated by the developing stroma (Fig. 9C). Stroma development seems to be most advanced in the central region, where collagen deposition is much thicker (Fig. 9C) compared to more peripheral regions where unfilled spaces in the stromal layer are widespread (Fig. 9D, E, G). The primary corneal epithelium has lost its scalloped appearance and is now formed of stratified squamous epithelial cells (Fig. 9N). These cells possess microvilli on the apical surface (Fig. 9N, arrowheads in O) and sit on a basement membrane located underneath the epithelium (Fig. 9P). Desmosomes are well formed at this stage in the intercellular junctions between epithelial cells located at the basal side (Fig. 9Q, arrowheads). In the developing stroma, collagen lamellae (arrowheads in Fig. 9R) were observed parallel with the cornea surface with keratocytes interspersed between the lamellae (Fig. 9R). Keratocytes have long thin processes running parallel to the collagen layers (Fig. 9R, T) with extensive intracellular networks of rough ER (Fig. 9S, T), possibly for the synthesis of collagen and proteoglycans. Collagen bundles were easily observed in the stromal layer and were occasionally seen inside the keratocyte cells (Fig. 9U). In endothelial cells, many fluid-filled vacuoles are present (Fig. 9V), possibly reflecting the endothelium's role in transporting fluid and solutes out of the cornea to maintain its transparency. Interestingly, we observed the presence of a slightly dark staining layer on top of the corneal endothelium (Fig. 9V, W), which could be the primary Descemet's membrane, and some collagen fibers were seen beyond this membrane (Fig. 9W). Three hours of EdU labeling indicated that the epithelial cells were undergoing proliferation and renewal whereas keratocytes and endothelial cells were rarely labeled (Fig. 9H–M), suggesting a very low division rate.

3.10. Stage 62 – dynamic change of the cornea associated with metamorphosis

Tail degeneration associated with metamorphosis starts at stage 62 and completes at stage 66. At stage 62, the cornea has finally detached from the lens and the lens has moved away from the retina (Fig. 10A, B). The lens zonules which connect the lens to the retina were not seen in the plastic section image.

Early in stage 62 we observed an unexpected epithelium-like cell mass, bulky in the center and thin on the periphery, within the stromal mass, separated from the outermost corneal epithelium by a very thin layer of stroma (Fig. 10I–M, N–P). The anterior epithelium from the previous stage, still continuous with the head epidermis, has thinned and now contains no more than 5 cell layers in the center (Fig. 10N), suggesting that the basal part of the epithelial layer might have been engulfed by the stroma. Dark

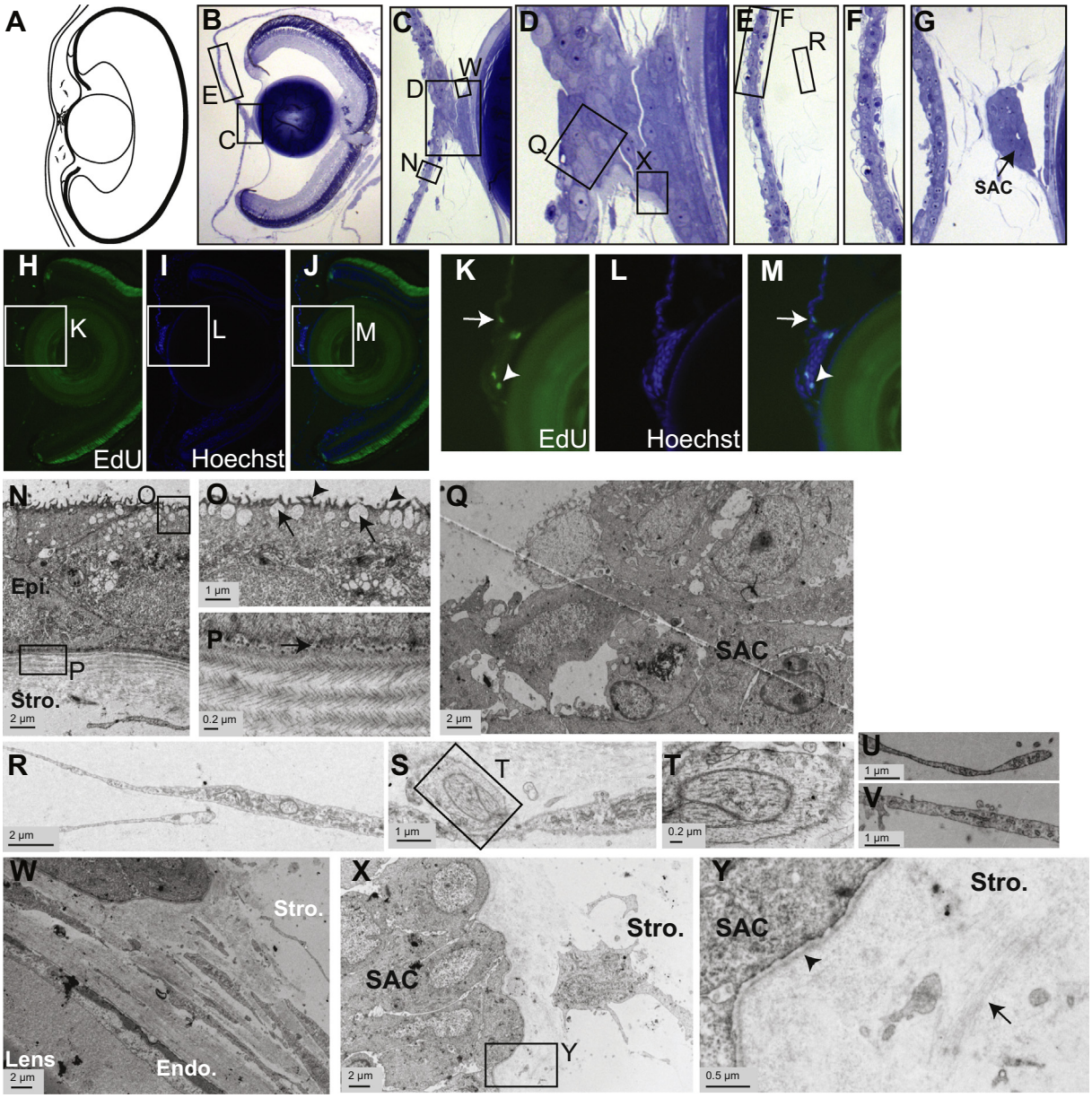

Fig. 7. *Xenopus* cornea at stages 48–50. (A) Schematic drawing of stage 48–50 eye. (B–G) Plastic section images of stage 48–50 eye (B), cornea (C), the SAC (D), the epithelium (E, F) and the SAC present in a different eye (G). (H–M) Proliferation assay showing dividing cells in the epithelium (arrow) and in the SAC (arrowhead). EdU (H, K), Hoechst (I, L), and overlaid (J, M). (N–Y) EM images of a plastic section adjacent to that displayed in panels B–F. (N) EM image showing the transitional epithelium and the anterior stroma. (O–P) Epithelial cells possess both microvilli (arrowheads) and vesicular structures (arrows) on the apical membrane (O) and are underlined by numerous dark staining particles (arrow in P). (Q) EM image showing anterior side of the SAC. (R–V) Details of the keratocytes. (T) High magnification image of one keratocyte containing a vesicle filled with short collagen fibrils. (W) EM image showing the posterior side of the SAC and the endothelium. (X–Y) EM images showing the lateral side of the SAC. Collagen fibrils are indicated by arrows and a boundary structure surrounding the SAC is marked by an arrowhead. Abbreviations: epi, epithelium; stro, stroma; SAC, stroma attracting center; endo, endothelium.

staining particles were observed in the boundary between anterior epithelium and anterior stroma (Fig. 10S) as well as between anterior stroma and the intra-stromal epithelial mass (Fig. 10T). The intra-stromal epithelial mass contains columnar epithelial cells homogenously from anterior side to posterior side (Fig. 10K, O and P). The stroma has increased in thickness (Fig.10Q, R). EdU labeling revealed proliferating cells in the epithelium (Fig. 10C–H).

In contrast in late stage 62 embryos we always observed a big space filled with some interesting structures, probably cellular debris, in the site previously occupied by the intra-stromal epithelial mass (Fig. 10U–Z), suggesting that massive apoptosis or autophagy might be taking place to replace the old structure with mature adult epithelium.

3.11. Stage 64–66 initial completion of frog cornea

The cornea has now completely separated from the lens (Fig. 11A–B). The intra-stromal epithelial mass is gone and is replaced by stratified corneal epithelium, (Fig. 11C–E) sitting atop a Bowman-like layer (arrow in Fig. 11F), as in the adult cornea. The corneal epithelium is going through extensive proliferation from stage 64 (Fig. 11D) to stage 66 (Fig. 11C), as evidenced by the significant increase in its thickness, while the thickness of the corneal stroma barely changes. At stage 66, the stroma is much thinner than the epithelium layer (Fig. 11C). However, clear and regular arrangement of collagen lamellae was observed (Fig. 11F), with the collagen lamellae closest to the epithelium being the thinnest. The

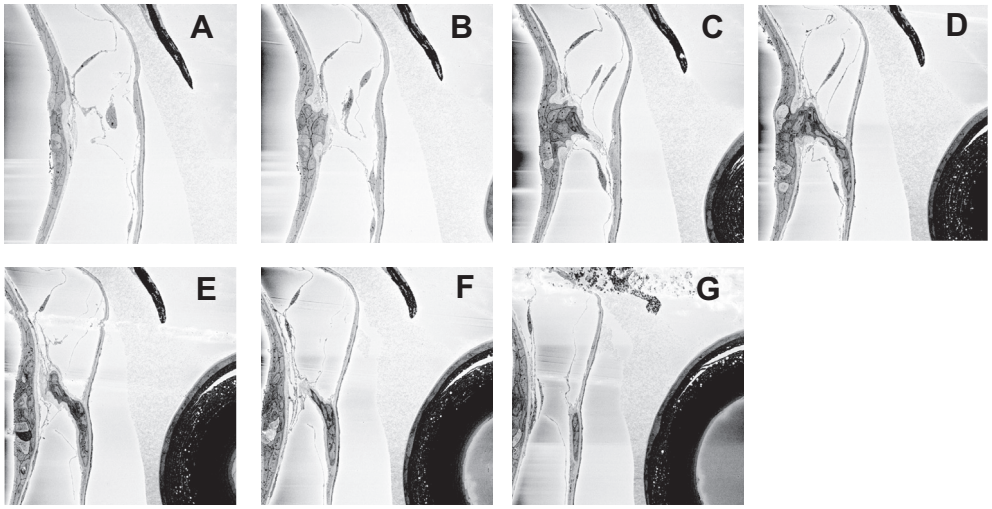

Fig. 8. Stroma attracting center in stage 48–50 cornea. (A–G) Selected EM images used in the 3D reconstruction of the SAC.

diameter of each collagen fibril is 0.04 μm. From this stage, the dorsal and ventral peripheral regions of the cornea start to show distinct structures. At the ventral side, the cornea is directly connected to the sclera but not connected to the epidermis (Fig. 11B). The lower eye lid is clearly observable for the first time (Fig. 11B). In contrast, the dorsal cornea is directly connected to both the sclera and the epidermis (Fig. 11B), indicating that there is no upper eye lid.

We performed EdU labeling for two different durations, 1.5 h and 12 h. Both protocols revealed labeled epithelial cells along the entire length of the corneal epithelium (Fig. 11I–N). Furthermore, endothelial cells (Fig. 11L) and keratocytes (data not shown) were occasionally labeled.

3.12. Adult cornea – maturation and maintenance of cornea

The cornea of a two-year-old adult *Xenopus* male consists of corneal epithelium, Bowman-like layer, corneal stroma, Descemet's membrane and corneal endothelium (Fig. 12A–C). The corneal epithelium, connected with the conjunctival epithelium but not the epidermis, is composed of about 13 layers of cells at the center and 10 layers of cells on the periphery. As a stratified non-keratinising epithelium, it contains cuboidal cells at the basal side (Fig. 12D, E) and flat squamous epithelial cells at the apical side (Fig. 12D, F). The corneal epithelium resides on a Bowman-like layer (Fig. 12G). Cells are connected to each other by mature junctional complexes (Fig. 12E, F).

In the adult corneal stroma, the collagen lamellae are arranged largely parallel to each other (Fig. 12H), but branching (Fig. 12J, K) and criss-cross patterns (Fig. 12I) were also frequently observed. In addition, we found that the collagen lamellae close to the epithelium were thinner compared to the ones further away (Fig. 12H). EdU staining showed some proliferating keratocytes (Fig. 13G–I).

Basal to stroma lies the Descemet's membrane (Fig. 12L), which is about 0.5 μm thick. The corneal endothelium is a single cell layer measured at approximately 1.4 μm in thickness (Fig. 12M) with intracellular fluid-filled vacuoles (Fig. 12L, N) and highly convoluted lateral margins (arrow in Fig. 12L). Endothelial cells were also occasionally labeled in proliferation assays (Fig. 13O–Q).

1.5 h, 3 h and 12 h EdU labeling all revealed proliferating epithelial cells along the entire length of the cornea. Interestingly, immunostaining revealed a pocket of cells positive for p63 in the peripheral region of the cornea (Fig. 13R–W), which has a wavy appearance. It is possible that this is the *Xenopus* equivalent of the human limbus, which might contain corneal stem cells that are responsible for repairing the cornea if injuries occur, while the proliferative cells in the basal epithelium are mainly responsible for routine maintenance and renewal.

To quantify the enlargement of the cornea during maturation we measured the total thickness of the cornea as well as the thickness of epithelium, stroma and endothelium separately from stage 60 to adult (Fig. 14). While stroma and endothelium do not change much except for a gradual increase in thickness (Fig. 14B), epithelium thickness exhibits a significant drop at stage 64 (Fig. 14B) probably due to the massive cell death observed in the intra-stromal epithelium during metamorphosis. After formation of the adult-like cornea at stage 64–66, the cornea still continues to thicken (Fig. 14A). This thickening is largely contributed by the stromal layer (Fig. 14B). At 2-years old, the stroma is around 70–80 μm thick and accounts for 65% of cornea thickness (Figs. 12C and 14B). The stroma layer consists of regularly arranged collagen lamellae and sparsely distributed keratocytes, most of which are positioned parallel to the collagen fibers (Fig. 12H). At stage 64–66, keratocytes are present at a density of about one per 100 μm^2. This density is maintained in the two-year-old cornea examined, suggesting that the increase in stromal thickness is likely due to continued synthesis of the collagen matrix.

4. Discussion

In this study, we investigated *Xenopus* corneal development from stage 25 to adult. Although the developmental process is largely conserved with that of the chick and mammals, we also found some features unique to *Xenopus* cornea, such as the multi-layered double cornea, the SAC, the intra-stromal epithelial mass observed during metamorphosis climax and massive cell death in this intra-stromal mass. The corneal morphogenesis is largely complete by the end of metamorphosis and the cornea continues to thicken thereafter. The adult *Xenopus* cornea is highly similar to human cornea in its structural composition, supporting its potential as a model system for human corneal diseases.

4.1. Dynamics of the interaction between inner cornea and lens

Around stage 30, the lens is induced from the basal layer of the embryonic epidermis (Fig. 1K). Following detachment of the lens

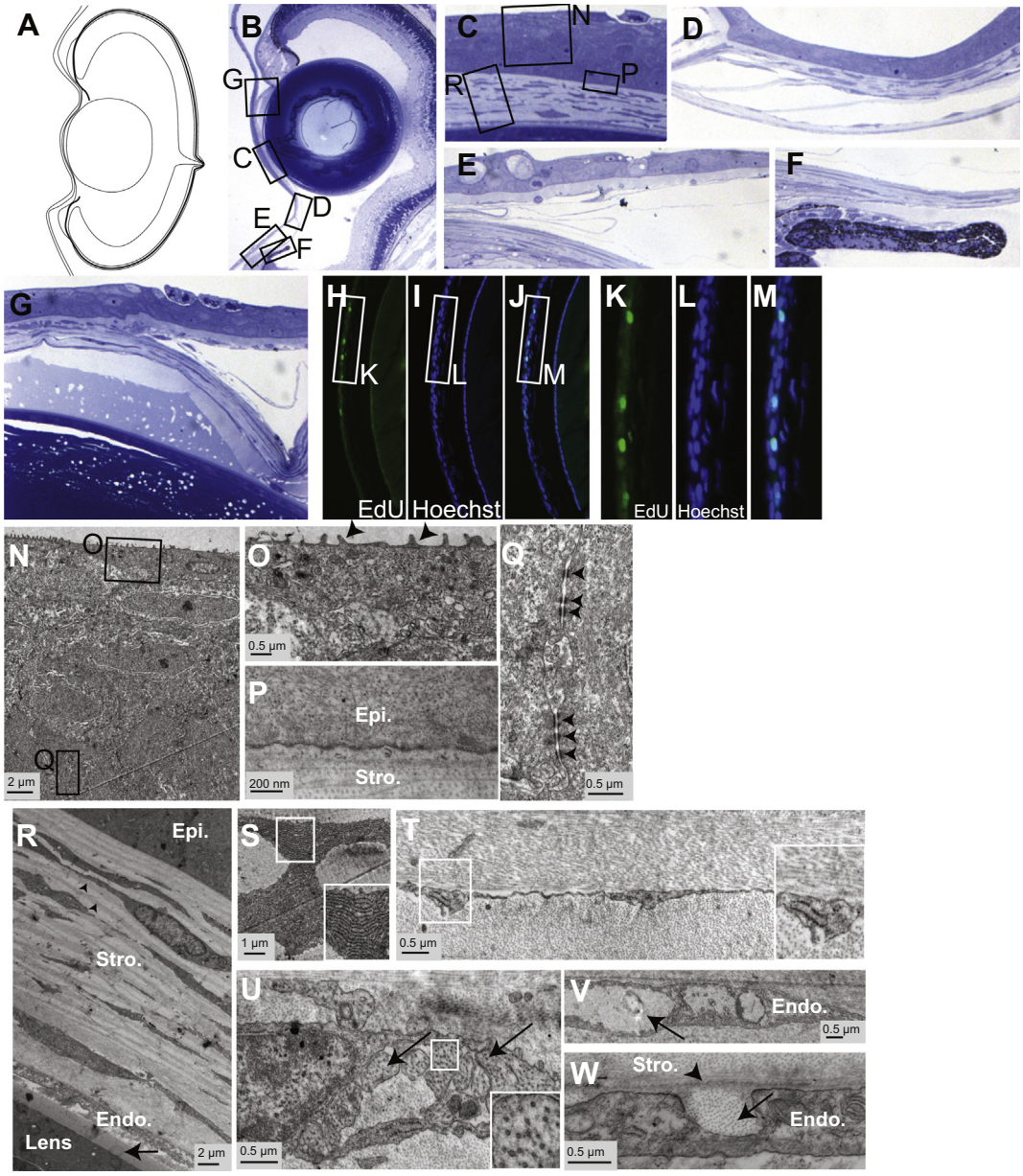

Fig. 9. *Xenopus* cornea at stage 55–60. (A) Schematic drawing of stage 55–60 eye. (B) Histology of stage 55–60 eye at low magnification. (C–G) Plastic section images of the different regions in the anterior part of the eye as indicated in (B). (H–M) Proliferation assay. EdU (H, K), Hoechst (I, L), and overlaid (J, M). (N–R) EM images of a plastic section adjacent to that displayed in panels B–G showing the primary corneal epithelium layer (N), the apical cell membrane (O), basement membrane (P) and intercellular junctions (Q). (R) EM image showing the corneal stroma and endothelium. (S–T) High magnification images showing the typical contents of a keratocyte (S), and the long and thin processes of a typical keratocyte (T). (U) Cross-sections of collagen fibrils (arrows) were occasionally observed in keratocytes. (V–W) EM images showing the developing corneal endothelium. In (V), intracellular vacuole is indicated by an arrow. In (W), arrow indicates a group of collagen fibers in the endothelial layer; arrowhead shows the presence of an early Descemet's membrane. Abbreviations: epi, epithelium; stro, stroma; endo, endothelium.

placode, mesenchymal cells migrate into the area between the basal epidermis and lens and form the presumptive corneal endothelium (Fig. 2B), which eventually develops into the corneal endothelium. Until stage 39, the presumptive corneal endothelium is attached to the embryonic basal epidermis (Fig. 3C). At stage 41, the presumptive corneal endothelium starts to separate from the embryonic epidermis (Fig. 4B), while still maintaining connection only at the center via a structure we name the stroma attracting center (SAC) (see below). At stage 43/45, the inner cornea is attached to the lens by an extracellular matrix layer (Fig. 5C). This attachment provides a large space between the outer cornea and the inner cornea for migration of keratocytes and the formation of the stroma (Fig. 7B). At stage 62, after initial filling of the stroma, the cornea separates from the lens (Fig. 10U). Thus, the development of the cornea proceeds through dynamic interactions between the corneal endothelium and the lens.

4.2. The stroma attracting center

In 1979, Bard and Abbott reported the unique connection between the corneal epidermis and the endothelium (Bard and Abbott, 1979). However, there has been no subsequent study of the structure and function. We have confirmed that the SAC is present in all embryos. It is initiated at stage 41 with a limited number of cells, and the cell number gradually increases. At stage 50, the three dimensional reconstruction of EM images revealed

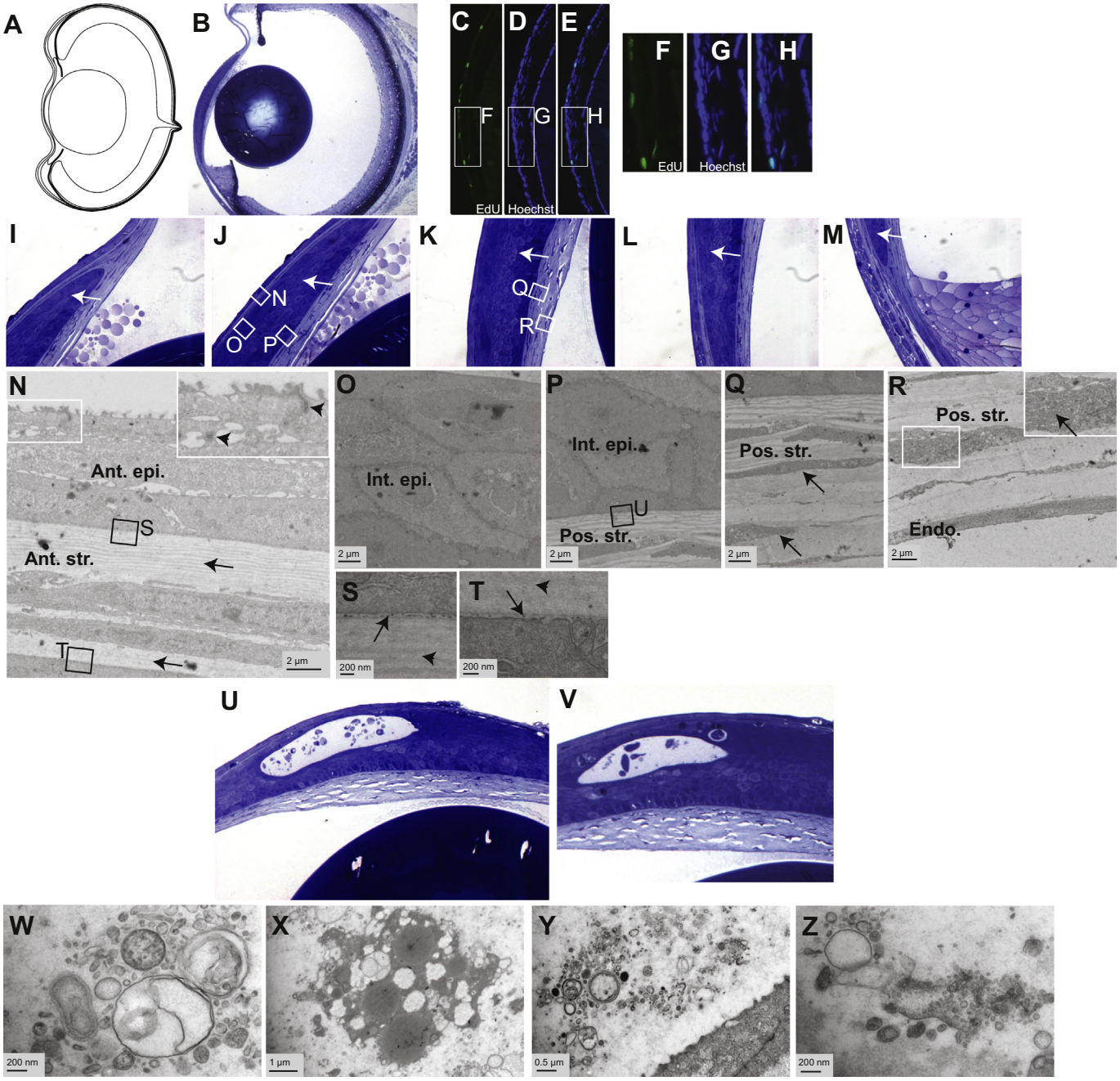

Fig. 10. *Xenopus* cornea at stage 62. (A) Schematic drawing of stage 62 eye. (B) Histology of stage 62 eye. (C–H) Proliferation assay. EdU (C, F), Hoechst (D, G), and overlaid (E, H). (I–M) Plastic section images of stage 62 cornea taken in dorsal to ventral order. The intra-stromal epithelial mass is indicated with arrows. (N–T) EM images of a plastic section adjacent to that displayed in panels I–M. (N) EM image showing the anterior epithelium and anterior stroma. Collagen fibers in the anterior stroma are indicated by arrows. Tight junctions (arrowheads) can be observed between anterior epithelial cells. (O–R) High magnification images of the intra-stromal epithelial mass (O), border of intra-stromal epithelial mass and posterior stroma (P), posterior stroma (Q), posterior stroma-endothelium border (R). Keratocytes (arrows in Q) lie parallel to the collagen lamellae and rough ER can sometimes be observed (arrow in R). (S–T) High magnification images showing dark staining particles (arrows) on the anterior epithelium-anterior stroma border (S) and the anterior stroma-intra-stromal epithelial mass border (T). Collagen bundles are indicated by arrowheads. (U–V) Plastic section images showing the apoptotic cells in the epithelium. (W–Z) EM image showing structures present in the apoptotic space. Abbreviations: ant epi, anterior epithelium; ant str, anterior stroma; int epi, intrastromal epithelium; pos str, posterior stroma; endo, endothelium.

that there were approximately 20 cells. Unlike the basal embryonic epidermis cells and the presumptive corneal endothelial cells, both of which are flat, the SAC cells are globular in shape (Fig. 4C), suggesting that they are a distinct cell type. Our study did not address the interesting question of the origin of cells in the SAC. However, as they are in direct contact with the epidermal cells but not with the presumptive endothelial cells (Fig. 8C, D), we speculate that they might be derived from the corneal embryonic epidermis.

After stage 50, the space between the epithelium and the endothelium is gradually filled by stroma. As shown in Fig. 8C–E, the SAC is surrounded by loosely-arranged keratocytes, some of which are in direct contact with SAC cells through their long processes. As the cell shape and cellular contents of the keratocytes and the SAC cells are markedly different, and the keratocytes are known to be originated from migrating NCCs, it is unlikely that keratocytes are derived from the SAC cells. Instead, we speculate

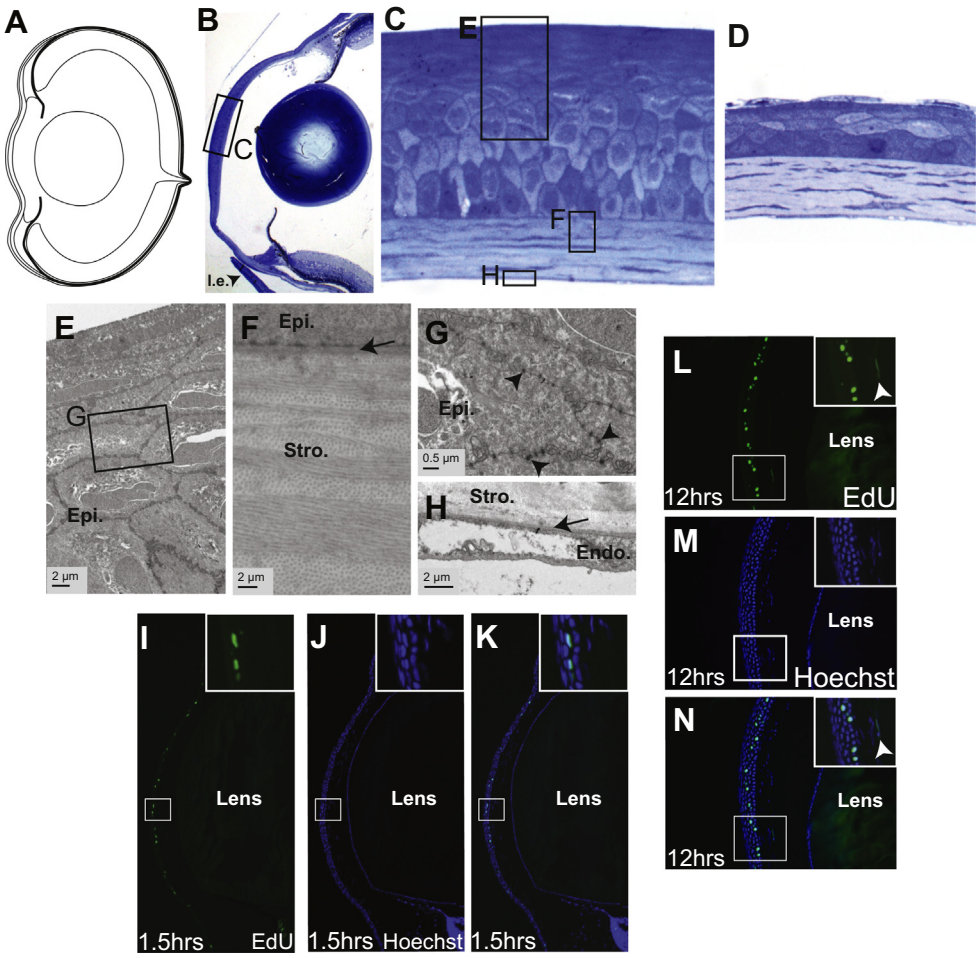

Fig. 11. *Xenopus* cornea at stage 64–66. (A) Schematic drawing of stage 64–66 eye. (B) Histology of stage 64–66 eye. (C–D) Plastic section images of stage 66 cornea (C) and stage 64 cornea (D) under the same magnification. (E–H) EM images of a plastic section adjacent to that displayed in panels B and C showing the cornea epithelium (E), and epithelium-stroma (F). Bowman like membrane is indicated by an arrow in (F). (G) High magnification image showing the intercellular connections in the epithelium (arrowheads). (H) EM image showing the stroma-endothelium border. Descemet's membrane is indicated by an arrow. (I–N) Proliferation assay for 1.5 h (I–K) and 12 h (L–N). EdU (I, L), Hoechst (J, M), overlaid (K, N). In (L) and (N) proliferative endothelium cell is indicated by arrowhead. Abbreviations: le, lower eyelid; epi, epithelium; stro, stroma; endo, endothelium.

that SAC might be secreting chemoattractants to attract keratocytes from the periocular space.

4.3. NCCs migrate into corneal endothelium and stroma

This study confirmed that, in *Xenopus*, the migrating NCCs contribute to the formation of the inner cornea, i.e. the corneal endothelium and keratocyte cells but not the corneal epithelial cells (Fig. 6). NCCs start migration at stage 20 and occupy the periocular space at stage 30 prior to entering the anterior chamber (Fig. 6B–D). As in chick and human, invasion of the migrating cell population into the cornea seems to occur in multiple waves. From stage 30 to stage 35, as the lens vesicle detaches from the overlying epidermis, the periocular mesenchyme invades to occupy the space between lens and epidermis. These migrating cells line up to form a monolayer that eventually develops into the corneal endothelium. The second migratory wave occurs from stage 41. Fibroblast-like cells invade the thin primary matrix underlying the epidermis and develop into the presumptive keratocyte layers of both inner and outer corneas. In this study, we confirmed that the inner cornea is derived from cells of neural crest origin, as the fluorescently labeled cranial NCC population was only observed in the inner cornea at stage 45 (Fig. 6H, M, 6P).

In addition, other optic structures such as the episcleral vasculature (Fig. 6N) seem to be labeled as NCC-derived as well, suggesting that the early migration may not be exclusively directed to the cornea. After this stage, migrated melanocytes are also established around the eye ball. The third wave of migration involves more fibroblast-like presumptive keratocytes (Fig. 8B–F). They are found most densely distributed around the SAC, which is likely to play an important role in attracting these migrating cells.

4.4. Initial stroma layer formation

The embryonic epidermis is underlined by extracellular matrix from stage 35 (Fig. 2I–J, 3J–J′ and 4I–J), within which the second migratory wave of NCCs invades. This indicates that this primary matrix may act as a required material for the future invasion to occur. The presence of numerous mitochondria (Fig. 2K) and extensive ER (Fig. 5M) in the basal epidermal cells indicates these cells contribute to the secretion of the primary stromal matrix.

4.5. Metamorphosis and lower eyelid opening

The mature adult *Xenopus* cornea consists of a stratified epithelial layer, a thick collagenous stroma interspersed with

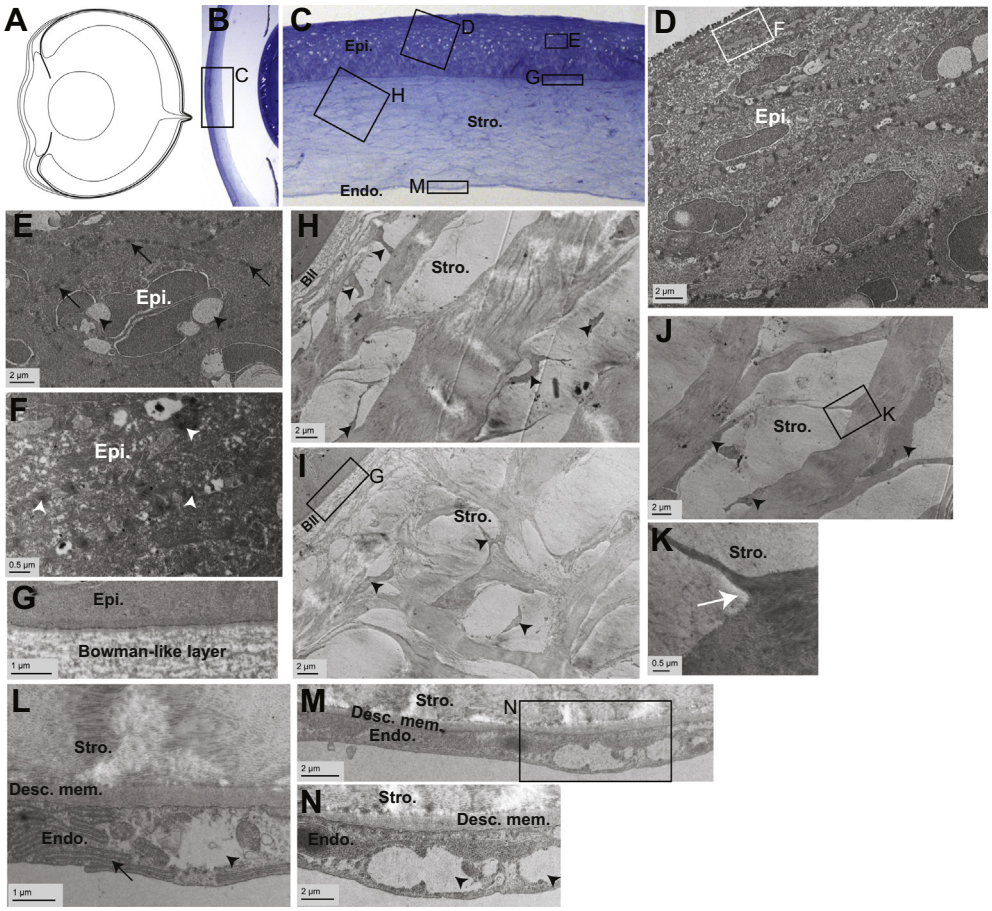

Fig. 12. Adult *Xenopus* cornea. (A) Schematic drawing of a 2 year-old adult eye. (B) Histology of the anterior segment of 2 year-old adult eye. (C) Plastic section image of the adult cornea. (D–N) EM images of a plastic section adjacent to that displayed in panels B and C. (D) EM image showing the mature epithelium. (E) High magnification image of one typical epithelial cell. Intercellular junctions are indicated by arrows and intracellular storage granules are indicated by arrowheads. (F) High magnification image of apical epithelial cells and the intercellular junctions (arrowheads). (G) EM image showing the basal epithelium and the Bowman-like layer. (H–I) EM images showing adult corneal stroma. Keratocytes are indicated by arrowheads. (J–K) High magnification EM images showing the arrangements of collagen fibers. In (J), keratocytes are indicated by arrowheads. In (K), the arrow indicates the branching point of a collagen fiber. (L–N) EM images showing Descemet's membrane and the endothelium containing fluid-filled vesicles (arrowheads). In (L), the arrow indicates the unique highly convoluted lateral membrane of a typical endothelial cell. Abbreviations: epi, epithelium; stro, stroma; endo, endothelium; Bll, Bowman-like layer; Desc.mem, Descemet's membrane.

numerous keratocytes and a single cell layered endothelium, together with two acellular layers, the Bowman-like layer and the Descemet's membrane.

Before reaching adult stage, *Xenopus* tadpoles start metamorphosis at stage 48 and finishes at stage 66. During this period, several tissues undergo active degeneration. We have found that the cornea also shows unique cell death. Firstly, an epithelial like cell mass surrounded by stroma is formed. Subsequently, massive cell death takes place in this intra-stromal epithelial mass (Fig. 10U–Z). We propose two hypotheses in regards to the origin of the intra-stromal epithelium. The first is that stroma invades into the corneal epithelium resulting in the isolation of a part of the epithelium inside the stroma. The second hypothesis is that the epithelial cells break the basement membrane and proliferate to form this structure inside the corneal stroma. We prefer the first hypothesis because we always observed massive cell death and cyst formation in the intra-stromal epithelium, possibly as a result of the normal migration of epithelial cells towards the cornea surface being blocked by the overlying stroma. Similar epithelial cysts have been described in human epithelial basement membrane dystrophy (Laibson, 2010), where the basal corneal epithelium is engulfed by the basement membrane resulting in cyst formation and cell death (Waring et al., 1978). Accompanying the massive epithelial death, the corneal thickness is markedly reduced (Fig. 14A, B).

Adult *Xenopus* has a lower eyelid but not an upper eyelid (Wiechmann and Wirsig, 2003). After stage 66, we can observe the opened lower eyelid (Fig. 11B), suggesting that the epithelial cell death might be associated with the process of eyelid opening.

Eyelid opening is a major event in cornea development (Zieske, 2004). It is associated with the differentiation and maturation of epithelium and stroma, as well as an alteration in the rate of cell proliferation in all corneal layers. Like eyelid opening in mammals, the appearance of the lower eyelid during the metamorphosis climax in *Xenopus* has similar correlations with the development of various corneal layers. For example, in human, prior to eyelid opening, the primitive corneal epithelium thickness is reduced from three-to-four cell layers thick to two cell layers and thickness only starts to increase significantly after eyelid opening. Similar reduction in epithelium thickness is also observed from stage 62 to stage 64 in *Xenopus* (Figs. 10K, 11D and 14B). The appearance of lower eyelid at stage 66 (Fig. 11B) is associated with the rapid thickening of the epithelium from stage 64 (Fig. 11D) to stage 66 (Fig. 11C), consistent with continued high proliferation rate observed in the epithelium during this development time window (Fig. 11I–N). Interestingly, stroma thickness drops slightly during the metamorphosis climax (Fig. 14B), possibly due to stroma dehydration by the fully differentiated and mature endothelium.

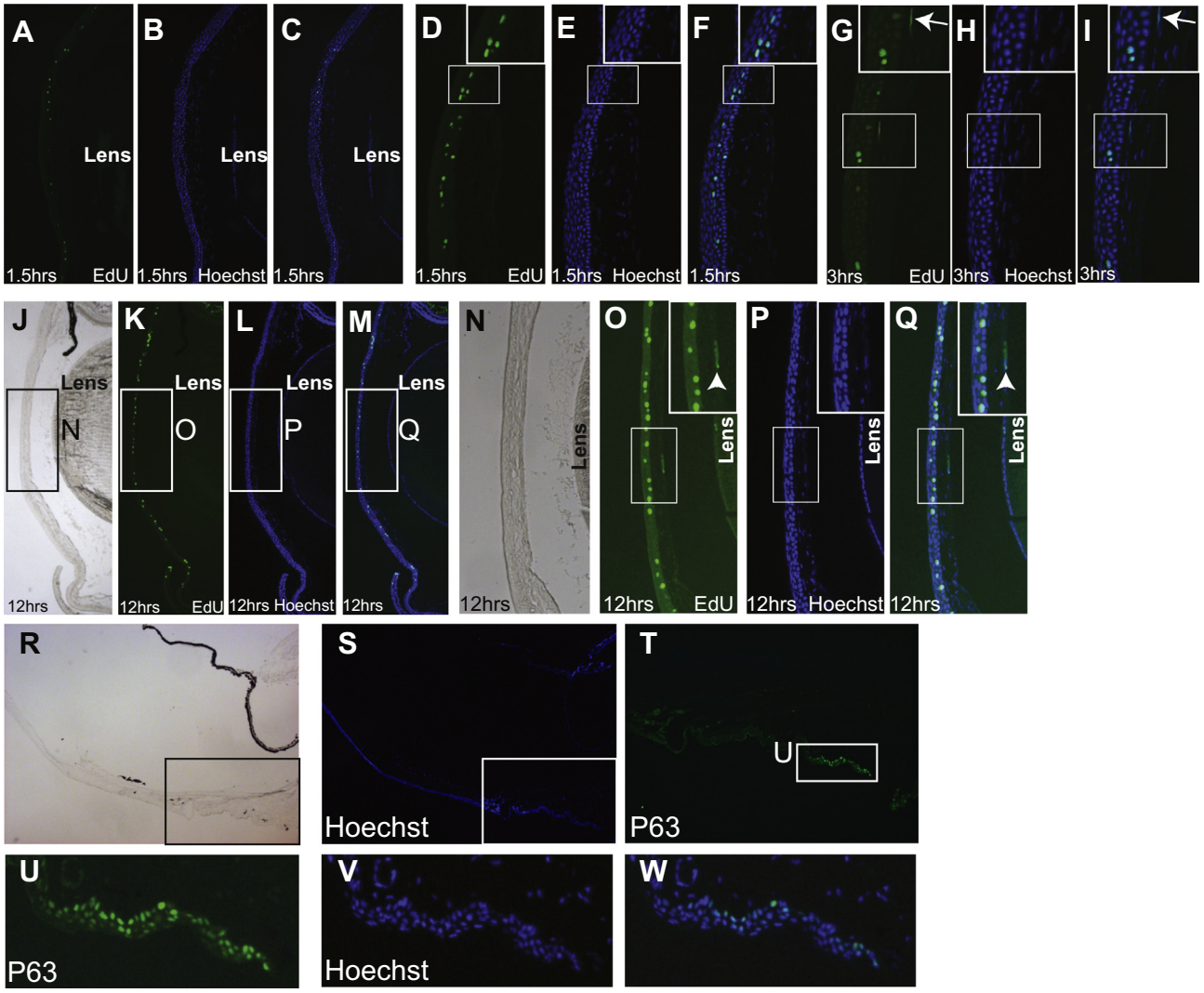

Fig. 13. Proliferative capacity of the cells in *Xenopus* adult cornea. (A–Q) Proliferation assays of 1.5 h labeling (A–F), 3 h labeling (G–I), and 12 h labeling (J–Q). Brightfield (J, N), EdU (A, D, G, K, O), Hoechst (B, E, H, L, P), overlaid (C, F, I, M, Q). In (G) and (I), proliferative keratocyte is indicated by an arrow. In (O) and (Q), proliferative endothelial cell is shown by an arrowhead. (R–W) Immunostaining of mature cornea using p63 antibody at low (R, S) and high (T–W) magnifications. Brightfield (R), p63 (T, U), Hoechst (S, V), overlaid (W).

4.6. Maturation of the corneal epithelium

Until stage 48/50, the apical embryonic epidermis consists of goblet cells, which have strong secretory activity, together with ciliated cells, which possess numerous cilia on the apical cell membrane. The embryonic corneal epidermis closely resembles epidermis elsewhere in the embryo. The goblet and ciliated cells are replaced by squamous corneal epithelial cells with apical microvilli in the mature *Xenopus* cornea (Fig. 9O). This transition takes place between stages 50 (Fig. 7) and 60 (Fig. 9) via an intermediate cell type that possess features of both embryonic and mature corneal epithelia, i.e. both secretory machinery and microvilli (Fig. 7N–O). Early stage *Xenopus* corneal epithelium has an ability to regenerate lens (Filoni, 2009; Henry and Tsonis, 2010). Interestingly, this lens regeneration capacity disappears after metamorphosis (Freeman, 1963), suggesting that possibly the embryonic epidermis is required for the regeneration.

4.7. The Bowman's layer and Descemet's membrane

Xenopus cornea has a Descemet's membrane between the stroma and endothelium (Fig. 12L). At stage 55/60, we could see the first sign of the Descemet's membrane as a distinctive dark layer sitting atop the corneal endothelium (Fig. 9W). It gradually thickens during and after metamorphosis. In mature cornea, its thickness is measured at approximately 400 nm (Fig. 12L).

In addition, we observed a Bowman-like layer in the mature *Xenopus* cornea composed of a loose network of collagen fibrils (Fig. 12G), distinctly different from the collagen arrangement in the stromal matrix. Its formation possibly starts at stage 64–66 where a thin matrix layer could be seen underneath the epithelial basement membrane (arrow in Fig. 11F). Previously it was believed that fish and amphibians do not possess a Bowman's layer. However, a study in zebrafish reported the presence of the Bowman's layer (Zhao et al., 2006). Our result suggests that *Xenopus* also has a Bowman-like layer in the cornea, similar to primates and some bird species.

4.8. Collagen lamellae structure

Xenopus adult stroma contains 8–9 lamellae, which are arranged largely parallel to each other (Fig. 12H), with some criss cross patterns observed too (Fig. 12I). The lamellae are composed of small diameter collagen fibrils (0.06 μm) with regular packing. The

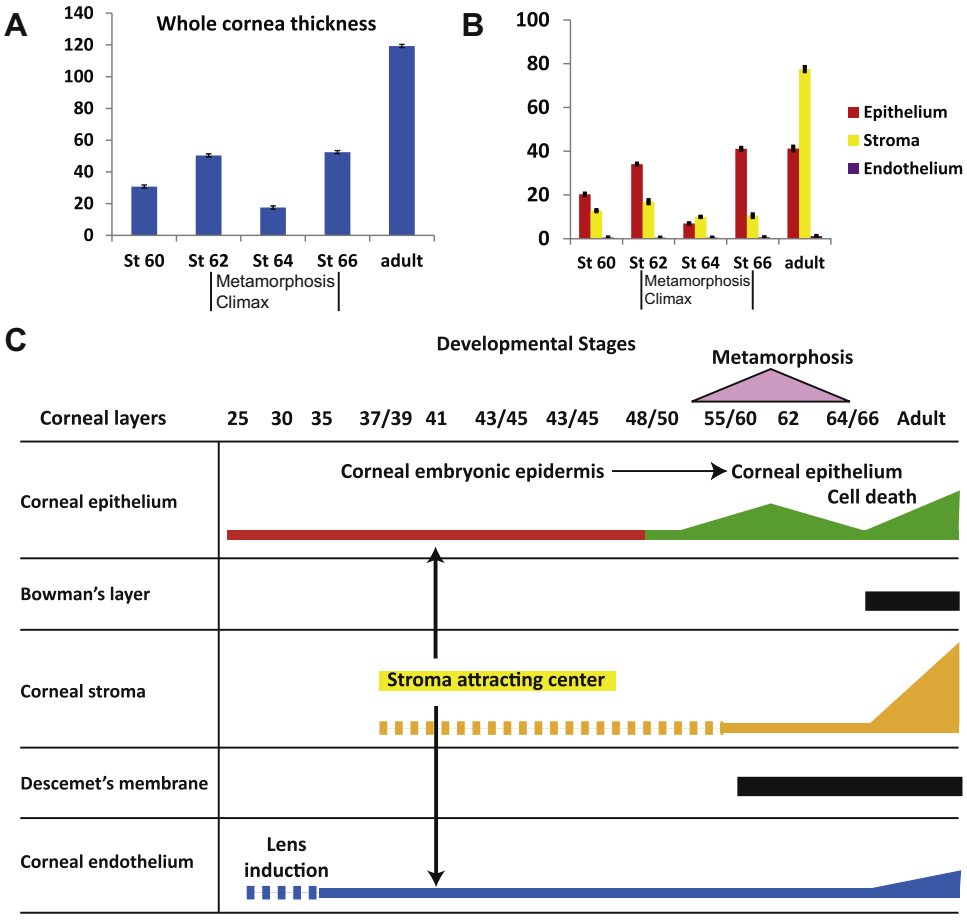

Fig. 14. Thickness measurement and summary of *Xenopus* cornea development. (A–B) Thickness measurement of the entire cornea (A) and separate layers (B) from stage 60 to adult. (C) Diagram summarizing the developmental timescale of all corneal layers. Thickness of the bars corresponds to the size of the tissue. Broken bar suggests periods of mesenchymal invasion in the formation of corneal stroma and endothelium.

collagen fibril diameter does not increase after stage 66. Most corneal keratocytes are oriented parallel to the adjacent lamella (Fig. 12J). Keratocytes have a compact cell body with numerous cytoplasmic lamellipodia, and a dendritic-like morphology. We did not observe a significant increase in keratocyte density in the cornea stroma during the maturation of the cornea.

4.9. The stem cells in adult Xenopus cornea

In adult *Xenopus* cornea, our analysis of cell proliferation shows some cells in the stroma and endothelium are dividing. This contrasts with mammalian cornea, in which there is no proliferation in adult stroma and endothelium, but is consistent with a recent study showing that mature chick corneal keratocytes still retain their proliferative ability and even some of the neural crest progenitor cell properties (Lwigale et al., 2005). The whole body of *Xenopus* continues to grow throughout life, i.e. a majority of organs retain growth potential during adulthood. For example, *Xenopus* adult retina has a stem cell niche at the most peripheral region of the retina, known as the ciliary marginal zone. The stem cells continue to provide neuronal and glial cells to the central retina throughout the life of the animal (Ohnuma et al., 2002). The proliferating cells in the corneal stroma and endothelium are probably required for the continuous growth of *Xenopus* cornea.

In adult mammalian cornea, the corneal epithelial cells are continuously being shed from the superficial layer and replenished so as to maintain the structure, thickness and transparency of the cornea. In order to explain this regeneration, two models have been proposed: the limbal epithelial stem cell model and the corneal epithelial stem cell model (Majo et al., 2008; Mort et al., 2012). At the most peripheral edge of the cornea, connecting with the conjunctiva, lies the limbus, which shows a unique wavy structure. Many studies have shown that the basal side of limbal epithelium has corneal stem cells (Kinoshita et al., 1981; Sadaghiani and Thiebaud, 1987; Schermer et al., 1986). The stem cells divide and provide transient amplifying cells, which move through the suprabasal layers to the basal layer of the corneal epithelium. There, the transient amplifying cells divide, then move up to the superficial layer and eventually are shed. On the other hand, the corneal epithelial stem cell model suggests the existence of stem cells at the basal corneal epithelial layer. A recent study proposes that in the case of normal maintenance of cornea, the corneal epithelial stem cells make a more significant contribution, while the limbus stem cells have an important role in restoring impaired cornea (Majo et al., 2008).

Our examination shows the presence of the limbus like region at the periphery of *Xenopus* cornea, which has a wavy structure and is positive for the limbus marker p63 (Fig. 13U). Our EdU analysis shows that the dividing cells are uniformly distributed at the basal corneal epithelium even though brief labeling (90 min) indicates that the basal cells, probably the transiently amplifying cells or the corneal epithelial stem cells, are dividing at the suprabasal region. All observations indicate that the system of corneal epithelial maintenance in *Xenopus* is highly conserved with that in mammals.

4.10. Potential of using Xenopus in cornea studies

So far, most of the studies in cornea and corneal diseases have been carried out using mammalian model systems such as mouse and rabbit. Although they are evolutionarily closer to human, such studies are often restricted by expensive cost, long development cycles and limit on animal number. Therefore, development of suitable models using more accessible lower vertebrate species such as frog and fish is required. In addition, because of their external development, critical stages of corneal morphogenesis such as mesenchyme invasion, formation of corneal endothelium, establishment of Bowman's and Descemet's membranes are more accessible in fish and frog for manipulations, imaging and drug testing than in chick, mouse and rabbit.

In this study, we provide evidence that the adult frog cornea is highly similar to that of the human cornea in terms of its layered structure. First, the *Xenopus* cornea contains all of the five layers found in the human cornea, including the corneal epithelium, stroma, endothelium and the two acellular layers, which are Bowman's layer and Descemet's membrane. Bowman's layer was previously thought to exist only in certain primate species and not found in lower vertebrates, but recent reports have clearly demonstrated its existence in zebrafish cornea (Soules and Link, 2005; Zhao et al., 2006). Here, we also present the micrographic evidence showing that subjacent to the corneal epithelium in the adult frog cornea, there is a Bowman-like layer composed of loosely-arranged collagen fibrils (Fig. 12G), distinctly different from the collagen arrangement in the stromal matrix. Second, in adult human cornea, the stroma layer accounts for more than 90% of the total thickness and the corneal epithelium accounts for less than 10% (Krachmer et al., 2011). Contrarily, mature zebrafish cornea features a very thick corneal epithelium making up approximately 60% of the total corneal thickness and a relatively thin corneal stroma (Zhao et al., 2006). Compared to zebrafish, the proportions of epithelium and stroma in frog cornea better resemble that found in human, with the corneal stroma accounting for more than 60% of the total thickness and the corneal epithelium accounting for the rest 40%. Lastly, this study has also demonstrated that the adult *Xenopus* corneal epithelium is being constantly renewed by the proliferating cells located in the basal layers of the corneal epithelium just like in the human cornea, and a limbal region might also exist in the peripheral cornea as a niche of corneal epithelium stem cells. Furthermore, *X. laevis* eyes are much bigger than zebrafish eyes, making manipulations such as injection, labeling and tissue grafting easier to be carried out in the frog.

Taking the advantages offered by the *Xenopus* system into consideration, we propose that *X. laevis* could serve well as a novel model organism for future studies in cornea and human corneal disease-related investigations.

5. Conclusion remarks

This paper investigates, in considerable detail, the process of *Xenopus* corneal development, which is summarized in Fig. 14. Despite some unique structures and processes, corneal morphogenesis in *Xenopus* is largely similar to that in other model organisms. In particular, the structure of adult *Xenopus* cornea is highly conserved to the mature human cornea, supporting its potential as a model system for studies of human corneal diseases. This work serves as a reference for any future work using the *Xenopus* cornea to study the basic mechanisms of corneal formation as well as the pathology of human corneal diseases.

Competing interests

The authors declare that they have no competing interests.

Authors' contributions

SO, WH and NH designed experiments and performed a majority of experiments. TK assisted EdU experiments. All authors have read and approved the manuscript.

Acknowledgments

We thank Drs. Julie Daniels, Andrew Quantock and Rob Young for reagents, helpful comments and critical reading of the manuscript. We thank Dr. Robert Mayor for technical assistance and Drs Stephen Bolsover and Margaret Dellett for critical reading of the manuscript. We acknowledge Ohnuma lab members for experimental assistance and encouragement. This work is supported by the Fight for Sight.

References

Aldave, A.J., 2011. The genetics of the corneal dystrophies. Dev. Ophthalmol. 48, 51–66.
Bard, J.B., Abbott, A.S., 1979. Matrices containing glycosaminoglycans in the developing anterior chambers of chick and *Xenopus* embryonic eyes. Dev. Biol. 68, 472–486.
Boch, J., Bonas, U., 2010. Xanthomonas AvrBs3 family-type III effectors: discovery and function. Annu. Rev. Phytopathol. 48, 419–436.
Carmona-Fontaine, C., Matthews, H.K., Kuriyama, S., Moreno, M., Dunn, G.A., Parsons, M., Stern, C.D., Mayor, R., 2008. Contact inhibition of locomotion in vivo controls neural crest directional migration. Nature 456, 957–961.
Coulter, H.D., 1967. Rapid and improved methods fr embedding biological tissues in Epon 812 and Araldite 502. J. Ultrastruct. Res. 20, 346–355.
Day, R.C., Beck, C.W., 2011. Transdifferentiation from cornea to lens in *Xenopus laevis* depends on BMP signalling and involves upregulation of Wnt signalling. BMC Dev. Biol. 11, 54.
Denk, W., Horstmann, H., 2004. Serial block-face scanning electron microscopy to reconstruct three-dimensional tissue nanostructure. PLoS Biol. 2, e329.
Dohlman, C.H., 1971. The function of the corneal epithelium in health and disease. The Jonas S. Friedenwald Memorial Lecture. Invest. Ophthalmol. 10, 383–407.
Doughty, M.J., 1990. Morphometric analysis of the surface cells of rabbit corneal epithelium by scanning electron microscopy. Am. J. Anat. 189, 316–328.
Filoni, S., 2009. Retina and lens regeneration in anuran amphibians. Semin. Cell Dev. Biol. 20, 528–534.
Freeman, G., 1963. Lens regeneration from the cornea in *Xenopus laevis*. J. Exp. Zool. 154, 39–65.
Gage, P.J., Rhoades, W., Prucka, S.K., Hjalt, T., 2005. Fate maps of neural crest and mesoderm in the mammalian eye. Invest. Ophthalmol. Vis. Sci. 46, 4200–4208.
Goldberg, J.S., Hirschi, K.K., 2009. Diverse roles of the vasculature within the neural stem cell niche. Regen. Med. 4, 879–897.
Henry, J.J., Tsonis, P.A., 2010. Molecular and cellular aspects of amphibian lens regeneration. Prog. Retin. Eye Res. 29, 543–555.
Ishibashi, S., Cliffe, R., Amaya, E., 2012. Highly efficient bi-allelic mutations rates using TALENs in *Xenopus tropicalis*. Biol. Open 1, 1273–1276.
Kanekar, S., Perron, M., Dorsky, R., Harris, W.A., Jan, L.Y., Jan, Y.N., Vetter, M.L., 1997. Xath5 participates in a network of bHLH genes in the developing *Xenopus* retina. Neuron 19, 981–994.
Kinoshita, S., Friend, J., Thoft, R.A., 1981. Sex chromatin of donor corneal epithelium in rabbits. Invest. Ophthalmol. Vis. Sci. 21, 434–441.
Koizumi, N., Okumura, N., Kinoshita, S., 2012. Development of new therapeutic modalities for corneal endothelial disease focused on the proliferation of corneal endothelial cells using animal models. Exp. Eye Res. 95, 60–67.
Krachmer, J.H., Mannis, M.J., Holland, E.J., 2011. Cornea and sclera: anatomy and physiology. In: Nishida, T., Saika, S. (Eds.), Cornea, third ed. Mosby, pp. 3–25.
Laibson, P.R., 2010. Recurrent corneal erosions and epithelial basement membrane dystrophy. Eye Contact Lens 36, 315–317.
Lei, Y., Guo, X., Liu, Y., Cao, Y., Deng, Y., Chen, X., Cheng, C.H., Dawid, I.B., Chen, Y., Zhao, H., 2012. Efficient targeted gene disruption in *Xenopus* embryos using engineered transcription activator-like effector nucleases (TALENs). Proc. Natl. Acad. Sci. U. S. A. 109, 17484–17489.
Linsenmayer, T.F., Fitch, J.M., Gordon, M.K., Cai, C.X., Igoe, F., Marchant, J.K., Birk, D.E., 1998. Development and roles of collagenous matrices in the embryonic avian cornea. Prog. Retin. Eye Res. 17, 231–265.
Lohman, L.E., Rao, G.N., Aquavella, J.V., 1982. In vivo microscopic observations of human corneal epithelial abnormalities. Am. J. Ophthalmol. 93, 210–217.
Lwigale, P.Y., Cressy, P.A., Bronner-Fraser, M., 2005. Corneal keratocytes retain neural crest progenitor cell properties. Dev. Biol. 288, 284–293.
Majo, F., Rochat, A., Nicolas, M., Jaoude, G.A., Barrandon, Y., 2008. Oligopotent stem cells are distributed throughout the mammalian ocular surface. Nature 456, 250–254.
Mort, R.L., Douvaras, P., Morley, S.D., Dora, N., Hill, R.E., Collinson, J.M., West, J.D., 2012. Stem cells and corneal epithelial maintenance: insights from the mouse and other animal models. Results Probl. Cell Differ. 55, 357–394.
Mussolino, C., Cathomen, T., 2012. TALE nucleases: tailored genome engineering made easy. Curr. Opin. Biotechnol. 23, 644–650.

Nakagawa, S., Brennan, C., Johnson, K.G., Shewan, D., Harris, W.A., Holt, C.E., 2000. Ephrin-B regulates the ipsilateral routing of retinal axons at the optic chiasm. Neuron 25, 599–610.
Nielsen, K., Hjortdal, J., Pihlmann, M., Corydon, T.J., 2013. Update on the keratoconus genetics. Acta Ophthalmol. 91, 106–113.
Nieuwkoop, P.D., Faber, J., 1967. Normal Table of *Xenopus laevis* (Daudin): a Systematical and Chronological Survey of the Development from the Fertilized Egg till the End of Metamorphosis. North-Holland Prb.Co.
Ohnuma, S., Hopper, S., Wang, K.C., Philpott, A., Harris, W.A., 2002. Co-ordinating retinal histogenesis: early cell cycle exit enhances early cell fate determination in the *Xenopus* retina. Development 129, 2435–2446.
Perron, M., Kanekar, S., Vetter, M.L., Harris, W.A., 1998. The genetic sequence of retinal development in the ciliary margin of the *Xenopus* eye. Dev. Biol. 199, 185–200.
Pfister, R.R., 1983. The effects of chemical injury on the ocular surface. Ophthalmology 90, 601–609.
Pinnamaneni, N., Funderburgh, J.L., 2012. Concise review: stem cells in the corneal stroma. Stem Cells 30, 1059–1063.
Pronych, S., Wassersug, R., 1994. Lung use and development in *Xenopus laevis* tadpoles. Can. J. Zool. 72, 738–743.
Sadaghiani, B., Thiebaud, C.H., 1987. Neural crest development in the *Xenopus laevis* embryo, studied by interspecific transplantation and scanning electron microscopy. Dev. Biol. 124, 91–110.
Schermer, A., Galvin, S., Sun, T.T., 1986. Differentiation-related expression of a major 64K corneal keratin in vivo and in culture suggests limbal location of corneal epithelial stem cells. J. Cell Biol. 103, 49–62.
Schmedt, T., Silva, M.M., Ziaei, A., Jurkunas, U., 2012. Molecular bases of corneal endothelial dystrophies. Exp. Eye Res. 95, 24–34.
Soules, K.A., Link, B.A., 2005. Morphogenesis of the anterior segment in the zebrafish eye. BMC Dev. Biol. 5, 12.
Stuart, P.M., Keadle, T.L., 2012. Recurrent herpetic stromal keratitis in mice: a model for studying human HSK. Clin. Dev. Immunol. 2012, 728480.
Theveneau, E., Mayor, R., 2011. Collective cell migration of the cephalic neural crest: the art of integrating information. Genesis 49, 164–176.
Walter, B.E., Tian, Y., Garlisch, A.K., Carinato, M.E., Elkins, M.B., Wolfe, A.D., Schaefer, J.J., Perry, K.J., Henry, J.J., 2004. Molecular profiling: gene expression reveals discrete phases of lens induction and development in *Xenopus laevis*. Mol. Vis. 10, 186–198.
Waring 3rd, G.O., Rodrigues, M.M., Laibson, P.R., 1978. Corneal dystrophies. I. Dystrophies of the epithelium, Bowman's layer and stroma. Surv. Ophthalmol. 23, 71–122.
West, J.B., Fu, Z., Deerinck, T.J., Mackey, M.R., Obayashi, J.T., Ellisman, M.H., 2010. Structure-function studies of blood and air capillaries in chicken lung using 3D electron microscopy. Respir. Physiol. Neurobiol. 170, 202–209.
Wiechmann, A.F., Wirsig, C.R., 2003. Color Atlas of *Xenopus laevis* Histology. Kluwer Academic Publishers.
Zhao, X.C., Yee, R.W., Norcom, E., Burgess, H., Avanesov, A.S., Barrish, J.P., Malicki, J., 2006. The zebrafish cornea: structure and development. Invest. Ophthalmol. Vis. Sci. 47, 4341–4348.
Zieske, J.D., 2004. Corneal development associated with eyelid opening. Int. J. Dev. Biol. 48, 903–911.